

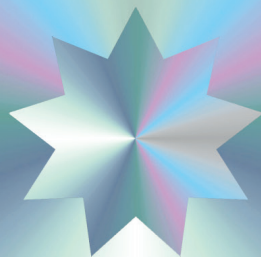


LIETUVOS  
ENERGETIKOS  
INSTITUTAS



Vilnius University  
Institute of  
Theoretical Physics  
and Astronomy

# Annual Report of the Association EURATOM / LEI



2013

ISSN 2029-1612 (print)

ISSN 2351-6976 (online)

© Lithuanian Energy Institute, 2014

## Content

Executive summary.....	4
General information .....	6
1 Safety Assessment of W7-X. Analysis of Loss-of-Coolant Accident.....	7
2 Limit Analysis of the W7-X Port Welds between the Plasma Vessel and the Ports .....	11
2.1 Models descriptions .....	11
2.2 Results of limit load analysis for port AEK20.....	15
2.3 Summary of the limit load analysis.....	21
3 Reliability analysis of W7-X divertor target cooling circuit and plasma vessel and ports cooling circuit.....	23
4 Activation cross sections for DD, DT and TT neutrons from JET plasmas .....	26
5 Activities in the frames of Power Plant Physics and Technology agreement.....	29
5.1 WP13-DTM-02: Reliability, Availability, Maintainability & Inspectability .....	29
5.1.1 WP13-DTM-02-T02: Method to evaluate and integrate diverse RAMI input data.....	29
5.1.2 WP13-DTM-02-T04: Analysis of the DEMO Availability Requirement.....	30
5.2 WP13-SYS-02: System level analysis.....	31
5.3 WP13-SYS-04: Safety .....	35
6 Calculations of spectroscopic characteristics for W ions.....	40
6.1 Investigation of the $4p^64d^N \rightarrow 4p^64d^{N-1}4f + 4p^54d^{N+1}$ excitation of highly charged $W^{+37}$ , $W^{+36}$ and $W^{+35}$ tungsten ions by electrons within Born approximation in quasi-relativistic approach with the correlation effects included.....	40
6.2 The evaluation of the accuracy of the theoretical investigation of ions with the different ionization degrees .....	41
6.3 Multiconfiguration Dirac-Hartree-Fock energy levels and transition probabilities for $W^{38+}$ .....	43
6.4 Application of the analogues of relativistic integrals in R-matrix method for highly charged tungsten ions.....	44
6.4.1 Introduction .....	44
6.4.2 Expressions for analogues of relativistic integrals.....	45
6.4.3 Results and discussion .....	45
6.5 References .....	49
7 Mobility program 2013 .....	50
8 Public information.....	53
9 Publications .....	54

## EXECUTIVE SUMMARY

Lithuanian Energy Institute (LEI) signed a contract on joining the European Fusion Development Agreement (EFDA) and starting from 1<sup>st</sup> January 2007 Lithuania officially became EFDA member. In 2013 EURATOM/LEI association successfully continued activities in research related to European Fusion Development Agreement activities. Our activities concentrate around three issues: Fusion safety issues, Plasma diagnostics and Technology development for burning plasmas.

The largest part of our activities is related to W7-X programme implemented by Max-Planck-Institut für Plasmaphysik (IPP) in Germany. In 2013 our association performed assessment of LOCA impact on W7-X Plasma Vessel internal structures, assessment of limit load analysis of the port welds as well as assessment of cooling circuit in case of loss of off-site power.

Assessment of W7-X Plasma Vessel venting system capacity was performed using computer codes RELAP5 and COCOSYS. RELAP5 was used to determine the mass and energy flow rates through the ruptured pipe and gas flows through the venting system. Detailed thermal-hydraulic model was developed to represent the complicated cooling system of W7-X. COCOSYS code was used for detailed analysis of Plasma Vessel.

The port welds between the Plasma Vessel and the ports in W7-X cryostat system was investigated and analysis was performed to define the limit load for welding connection between the port AEK20 and the PV shell with gap 1 mm. The welding efficiency for analysis was assumed 0.7 and 0.85. The received results showed that limit loads are significantly higher than expected loads during operation, thus the integrity of the welding will be ensured.

The reliability analysis of the W7-X plasma vessel and ports cooling circuit ABK10 and the divertor target cooling circuit ACK10 were performed. The total unavailability and its main contributors are identified for “baking” and plasma operation modes.

In 2013 Lithuanian Energy Institute participated in JET task JW13-FT-5.54 Activation cross sections for DD, DT and TT neutrons from JET plasmas. The goals of the present task were the following: 1) Assess and update the activation cross sections used in JET neutron diagnostics both at 2.5 and 14 MeV neutron energy in view of the DT campaign, with particular regard to the related uncertainty in typical JET neutron spectra, and 2) Investigate suitable activation cross sections for measuring the TT neutron spectrum. Assess the related uncertainty.

In 2013 our association continued activities in the frames of EFDA WP 2013 in the following tasks:

- o Design Tools and Methodologies WP13-DTM-02 “Reliability, Availability, Maintainability & Inspectability (RAMI)”. LEI was involved in:
  - WP13-DTM-02-T02: Method to evaluate and integrate diverse RAMI input data
  - WP13-DTM-02-T04: Analysis of the DEMO Availability Requirement.
- o System Codes WP13-SYS-02 System Level Analysis,
  - WP13-SYS-02-T08: Activation and radiation dose map calculation.
- o System Codes WP13-SYS-04 Safety,
  - WP13-SYS-04-T05: Review of modelling codes and identification of development needs.

Tungsten as a heat-resistant material is planned to be used for ITER. Using tungsten in some parts of the tokamak may solve the tritium retention problem. On the other hand, tungsten atoms can detach from the inner walls of the fusion reactor, penetrate into the plasma and be ionised to very high degrees. Various tungsten ions will irradiate strongly thus cooling the plasma. Our association performed theoretical studies of the spectroscopic characteristics of highly charged tungsten atoms having open d and f-shells accounting for relativistic and correlation effects. These results could contribute to development of plasma diagnostic techniques in the future.

The total research volume of the 2013 activities was ~8 professional man-years.

## GENERAL INFORMATION

### EURATOM/LEI Steering Committee

#### European Commission

Mr. Simon Webster, Head of Unit – K6 G.6 (Fusion Energy)

Mr. Angelgiorgio Iorizzo, Research Programme Officer, G.6 (Fusion Energy)

Mr. Marc Cosyns, Administrator RTD – G.7 (Administration and Finance)

#### Lithuania

Mr. Romualdas Kisielius (Vilnius University Institute of Theoretical Physics and Astronomy)

Mr. Liudvikas Pranevičius, Vytautas Magnus University

Mr. Stanislovas Žurauskas, Ministry of Education and Science

### EURATOM/LEI Head of Research Unit

Eugenijus Ušpuras

Lithuanian Energy Institute

Breslaujos g. 3, LT-44403 Kaunas, Lithuania

Phone: +370 37 401926

Fax: +370 37 351271

e-mail: [uspuras@mail.lei.lt](mailto:uspuras@mail.lei.lt)

### Research Unit in Lithuania

#### Lithuanian Energy Institute

Breslaujos g. 3, LT-44403 Kaunas, Lithuania

Phone: +370 37 401801

Fax: +370 37 351271

e-mail: [rastine@mail.lei.lt](mailto:rastine@mail.lei.lt)

URL: <http://www.lei.lt>

#### Vilnius University Institute of Theoretical Physics and Astronomy

A. Goštauto g. 12, LT-01108 Vilnius, Lithuania

Phone: +370 5 2193251

Fax: +370 5 2125361

e-mail: [tfai@tfai.vu.lt](mailto:tfai@tfai.vu.lt)

URL: <http://www.tfai.vu.lt>

# 1 SAFETY ASSESSMENT OF W7-X. ANALYSIS OF LOSS-OF-COOLANT ACCIDENT

The principal investigators for this task are E. Urbonavičius, M. Povilaitis, and T. Kaliatka of LEI.

Rupture of the 40 mm pipe in the plasma vessel of W7-X during operation mode “baking” is considered as the most dangerous loss-of-coolant accident (LOCA). Before the investigations of this accident was performed neglecting the availability of the in-vessel components. In reality the pipe rupture would occur in the space behind the baffle and divertor, thus the flow area for the steam to the main volume of plasma vessel would be limited. This could have an impact on the pressurisation rate of the plasma vessel and impose loads on the in-vessel components. The model was developed and LOCA analysis was performed taking into account these in-vessel components.

The nodalisation scheme of W7-X Plasma Vessel venting system is presented in Figure 1.1. The volume of each node and the associated areas of the structures connected to the nodes are presented as well. The red lines show junctions between the nodes for atmospheric flow, and the blue arrows indicate the flow of water, which appears due to steam condensation.

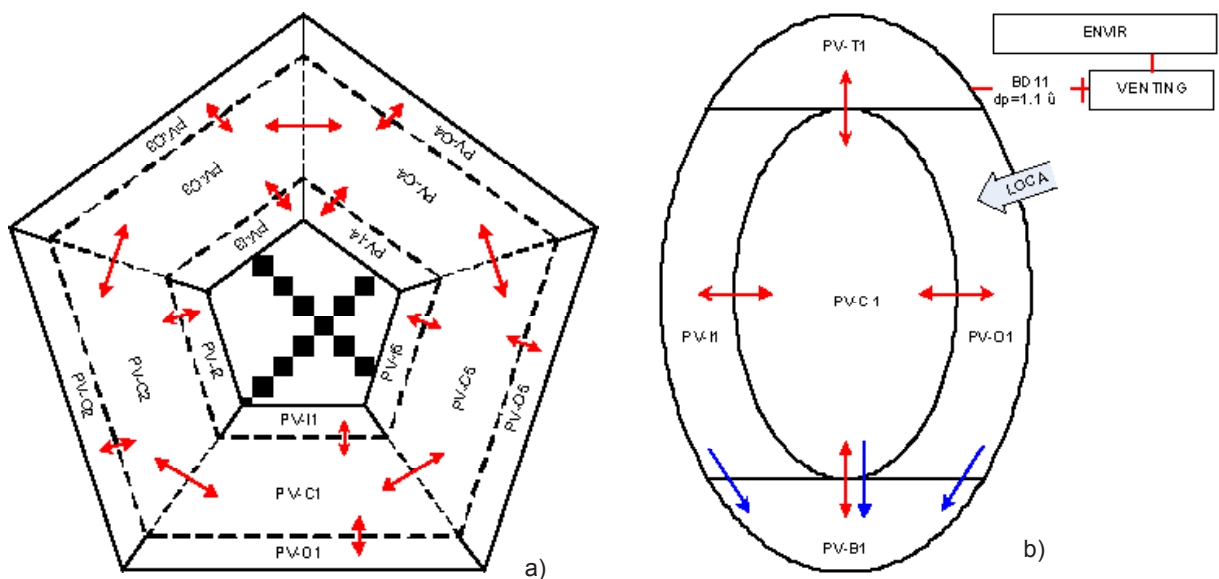


**Figure 1.1**

Nodalisation scheme of W7-X Plasma Vessel for COCOSYS: a) – top view; b) – cross section view

The outer surface of structure associated with this node faces the outside environment, which could have temperature different from the temperature inside the building. For the base case analysis it was assumed that the temperature in the outside environment is also 20 °C.

The structures of the plasma vessel were assumed to be hot with temperature of 150 °C. Such temperature is constant during the entire calculation time. Since COCOSYS code cannot simulate

deep vacuum conditions, it is assumed that the initial pressure inside plasma vessel is 1000 Pa, which is the lowest possible pressure possible in the code.

The analysis of the loss of coolant accident scenario, which assumes 40 mm diameter pipe rupture in the operation mode “Baking”, was performed. During this operation mode, the inner surfaces in the plasma vessel are cleaned from impurities and plasma vessel is prepared for plasma ignition. The coolant release rate and the specific enthalpy of the released coolant were calculated using RELAP5 code and are shown in Figure 1.2. After pipe rupture the maximal flow rate through the break into the plasma vessel reaches ~28 kg/s, but after this peak it gradually decreases. This decrease is related to closure of the automatic valves in the baking circuit. After 25 s the release rate to the plasma vessel is ~5 kg/s and after 80 s it is < 2 kg/s. The specific enthalpy of the released coolant changes with the time – at first only water is released but after ~75 s the superheated steam appears.

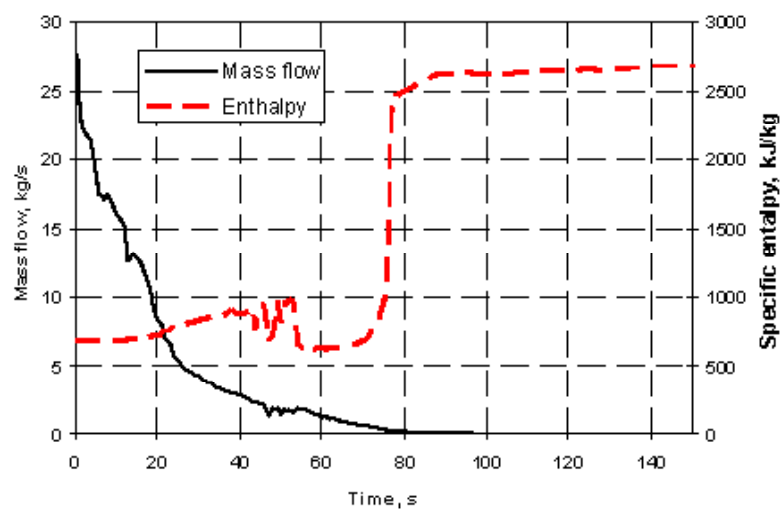


**Figure 1.2**  
Coolant release rate and specific enthalpy to plasma vessel received from RELAP5 code analysis

In the analysis the following assumptions were made regarding the flow areas through the gaps of the internal structures:

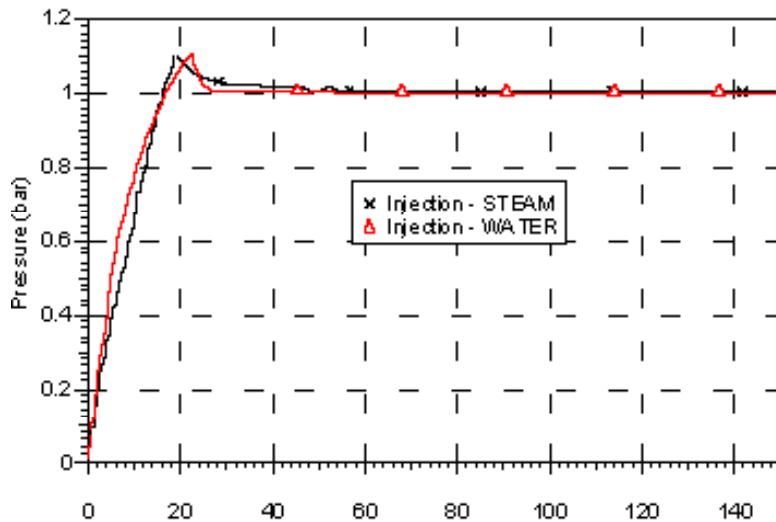
- o PV-C1 -> PV-T1 area 0.2 m<sup>2</sup>;
- o PV-C1 -> PV-B1 area 0.2 m<sup>2</sup>;
- o PV-C1 -> PV-I1 area 0.62 m<sup>2</sup>;
- o PV-C1 -> PV-O1 area 0.08 m<sup>2</sup>.

The diameter of the burst disk in the plasma vessel venting system is 250 mm.

The base case analysis is performed assuming that all system operate as designed. As well it is assumed that the ruptured pipe is in the same module as the connected pipe of the plasma vessel venting system.

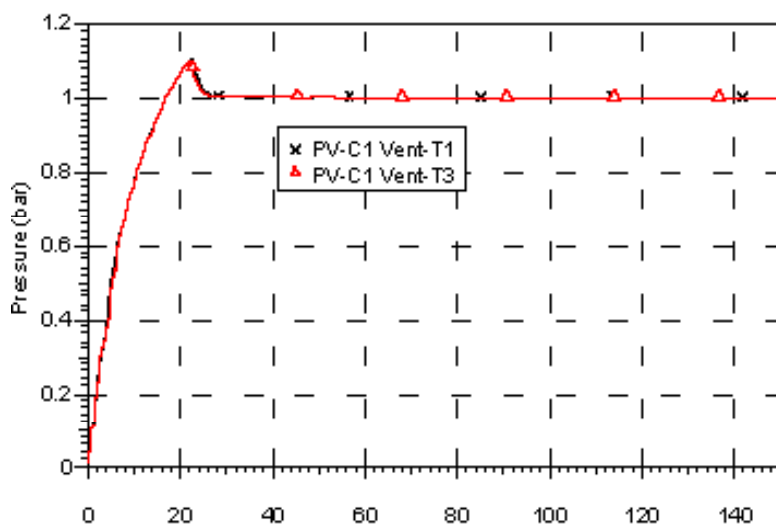
Figure 1.3 presents how the pressure in the nodes changes during the accident. Two types of coolant injection are possible to assume in COCOSYS: water or steam. This assumption has important influence on the results. If most of coolant is injected as water then burst disk opens 22.7 s if as steam then 19 s. However, in both cases rupture disk capacity is enough to prevent overpressure.

To investigate the influence of the break location on the received results, an additional variant calculation was performed assuming that the rupture is located in Module 1, but the plasma vessel venting system is connected to Module 3. In the base case scenario, it was assumed that the



**Figure 1.3**  
Pressure in the nodes

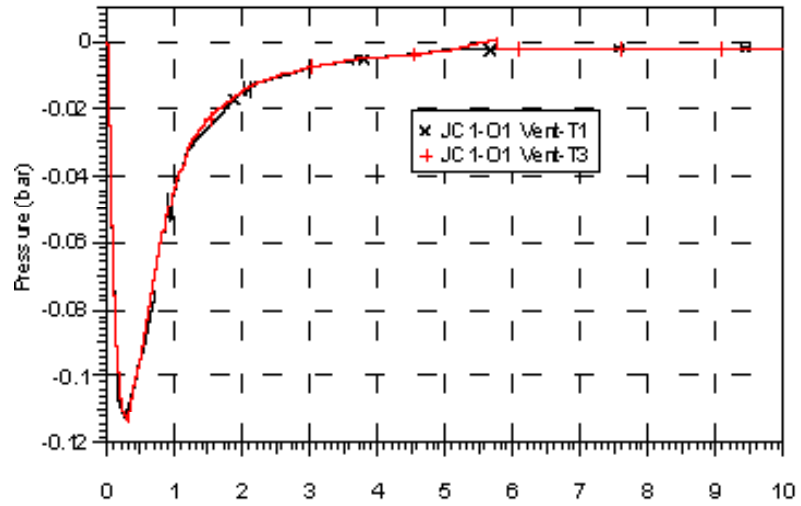
ruptured pipe and venting system are connected to the same module. The results of the analysis are presented in Figure 1.4. It is seen that the influence of the rupture location in relation to the venting system has only minor influence.



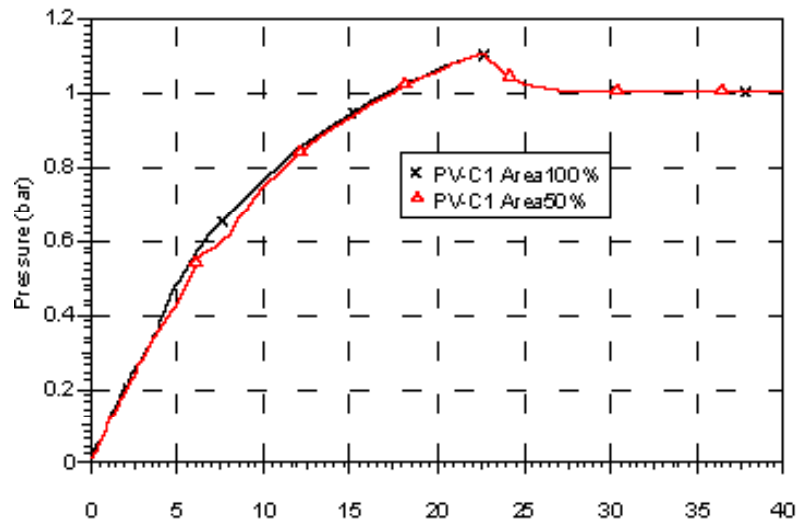
**Figure 1.4**  
Influence of rupture location: Pressure in nodes

Figure 1.5 presents the pressure difference on internal structures for two calculated cases: 1) base case, and 2) assuming the ruptured pipe and venting system are connected to different modules. In both cases the pressure difference is  $\sim 0.11$  bar, thus the rupture location does not have significant influence neither on the total pressure, nor on the pressure difference on the internal structures.

The flow area through the internal structures is not exactly known; therefore, additional calculations to investigate the influence of this parameter on the results were performed. Figure 1.6 shows the comparison of pressure in plasma vessel for base case scenario with variant assuming 50% reduction of the flow area. The calculated results show that there is no significant influence on the total pressure. However, there is significant influence on the pressure difference on the internal structures (Figure 1.7). The pressure difference on the internal structures increases to 0.23 bar as compared to 0.11 bar in the base case.



**Figure 1.5**  
Pressure difference on internal structures



**Figure 1.6**  
Influence of flow area: Pressure in PV

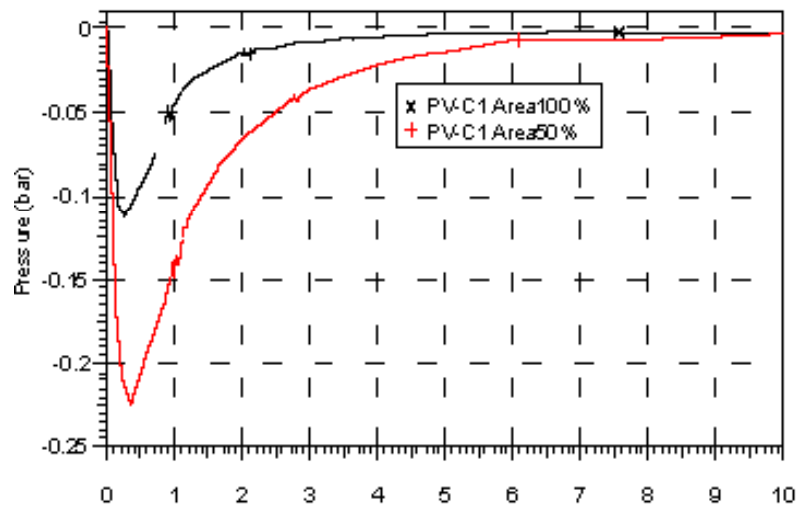


**Figure 1.7**  
Influence of flow area: Pressure difference on internal structures

## 2 LIMIT ANALYSIS OF THE W7-X PORT WELDS BETWEEN THE PLASMA VESSEL AND THE PORTS

The principal investigators for this task are G. Dundulis and R. Janulionis of LEI.

The load scale limit analysis to failure of the welding connections for ports AEK20 and the PV shell with gap 1 mm was performed. For the geometrical modelling CAD software SolidWorks was applied. Prepared geometrical model was transferred to FE software ABAQUS. These ports were modelled using the FEM technique as 3D bodies together with the regions of the PV shell around the ports and the welding seam. The models were loaded with forces, moments, and pressure provided by Max Planck Institute of Plasma Physics (IPP) staff and subjected to the load scale limit analysis. The main objective of this analysis is calculating limit load scaling factors. The analysis of port weld AEK20 with a 1 mm gap and 3 versions of calculating step were performed using ABAQUS code.

### 2.1 Models descriptions

This section contains port model AEK20 descriptions. Details of the port and weld seams geometry have been described in the report “Request for Limit Analysis of Port Welds between the Plasma Vessel and the Ports in the W7-X Cryostat System”.

The modelling of the welding connection between the port AEK20 and the PV shell was performed in two steps. In the first the geometrical 3D models of these port welds were prepared using the software SolidWorks. The prepared models are presented in Figure 2.1 – Figure 2.4. These models were transferred to FE software ABAQUS/Standard. The finite element models of the welding connection between the port AEK20 and the PV shell was prepared using this software. The prepared models are presented in Figure 2.2 and Figure 2.3. Model of port connection consist of

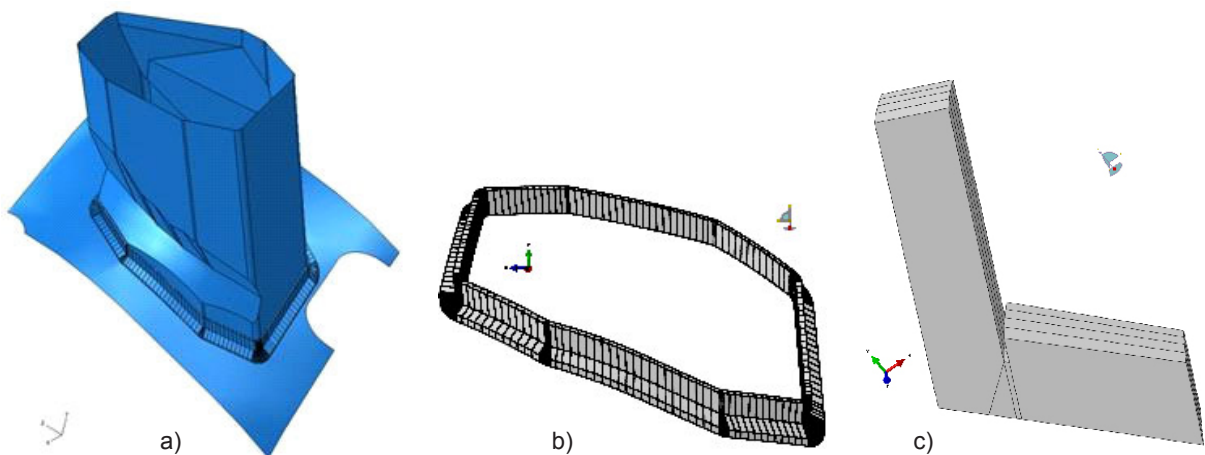


**Figure 2.1**

Geometrical model of the welding connection between the port AEK20 and the PV shell with 1 mm gap: a) – weld and around it port and vessel model, b) – central part solid model (Port, PV, weld seam), c) – cross section of central part

a shell modelled portion PV, a port, and a solid modelled central part (CP). Central part includes a portion of PV and a port and a full weld seam (see Figure 2.2, b).

For modelling of port AEK the linear 4-node shell elements with reduced integration S4R for shell parts of port and quadratic eight node shell elements with reduced integration S8R of the shell

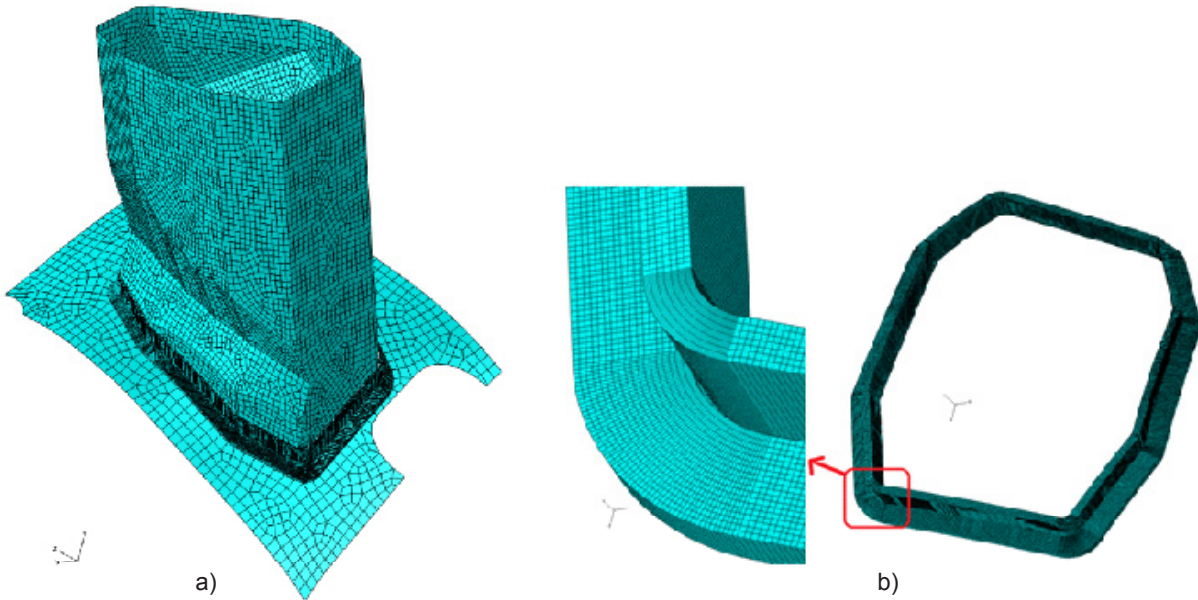


**Figure 2.2**

FE model of the welding connection between the port AEK20 and the PV shell with 1 mm gap:  
 a) – weld and around it port and vessel model, b) – close view of CP meshing

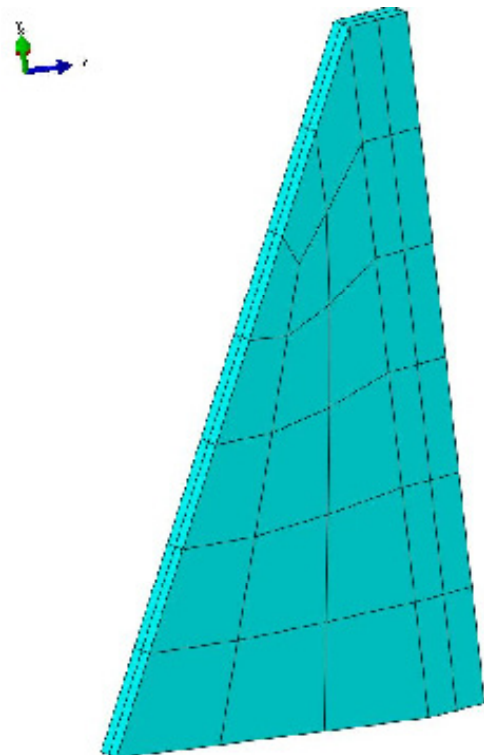


**Figure 2.3**

Cross sectional view of AEK20 1 mm gap weld seam meshing calculating version v1, v2

part of PV (see Figure 2.2, a) were used. Central part, part of plasma vessel and port (see Figure 2.2, b) are modelled as solid, are meshed using a 20-node quadratic brick element with reduced integration C3D20R. Weld seam is meshed using a 20-node quadratic brick element integration C3D20 (see Figure 2.3).

The PV shell and the ports are made of the material WS-Nr. 1.4429. The welding material is WS-Nr. 1.4455. The geometrical and material data of the welding connection between the port AEK20 and the PV shell are presented in Table 2.1. The names of the port welds parts used in Table 2.1 are presented in Figure 2.4.

**Table 2.1** Material properties

<i>Property</i>	<i>T, °C</i>	<i>Shell-AEK-1</i>	<i>Shell-AEK-2</i>	<i>Shell-AEK-3</i>
Thickness, mm	–	16.05	14.05	4.3
Density, kg/mm <sup>3</sup>	0–100	2.0511×10 <sup>-05</sup>	1.1513×10 <sup>-5</sup>	1.3214×10 <sup>-5</sup>
Young modulus, MPa	0	1.98×10 <sup>5</sup>		
	20	1.96×10 <sup>5</sup>		
	100	1.90×10 <sup>5</sup>		
Poisson's ratio	0–100	0.3	0.3	0.3
Coefficient of thermal expansion, K <sup>-1</sup>	0	1.60×10 <sup>-5</sup>		
	20	1.61×10 <sup>-5</sup>		
	100	1.67×10 <sup>-5</sup>		

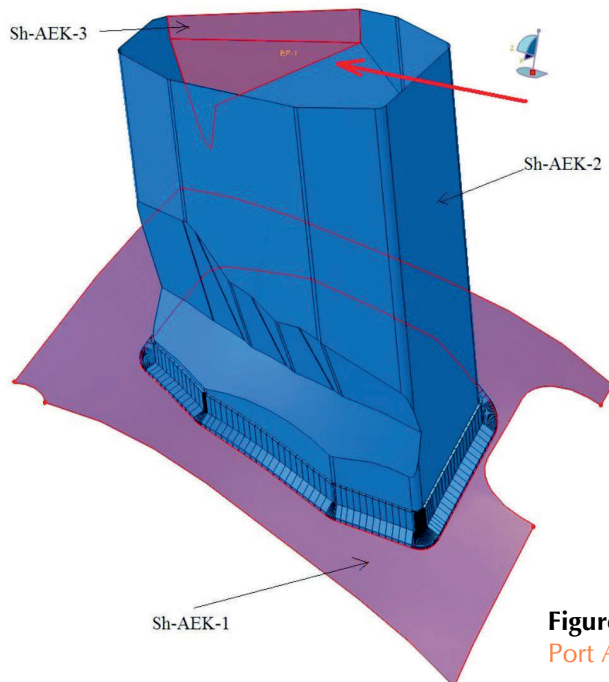


**Figure 2.4**  
Port AEK20 and the PV shell around it

In order to calculate limit load scaling factors, the outer boundaries of the PV (marked red) were constrained in the following way, the displacements of the edges were restricted in all directions, but rotations are allowed.

Restrained edges of models shells are highlighted in Figure 2.5.

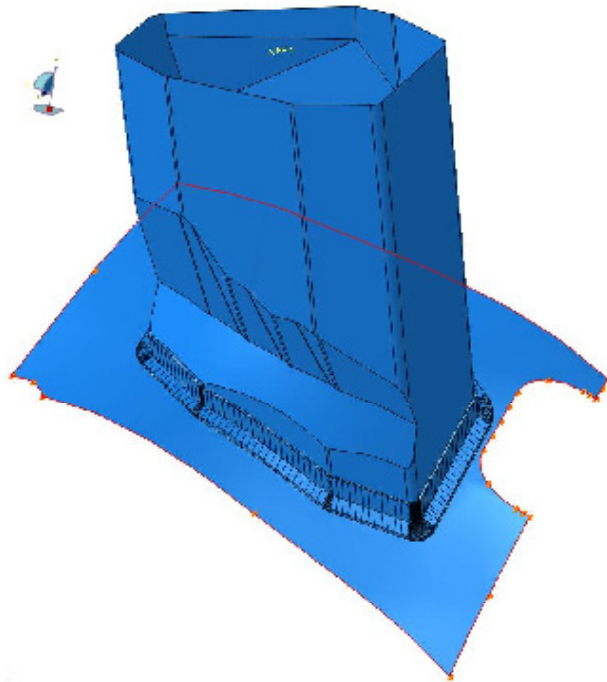


**Figure 2.5**  
FE model boundary conditions Port AEK

The loads were applied at the loading step that corresponds to the loading factor of 1.0 are listed in Table 2.2. “Outer pressure” means that the pressure is applied from the side where the port is attached to the PV shell. The loads are multiplied with the safety value of 1.2 in order to take possible imprecision of the modelling into account. Safety value of 1.2 is not applied to gravity.

**Table 2.2** Loads on the sub-model for the LC 5

<i>Load type</i>	<i>Direction</i>	<i>Port AEU30</i>
Temperature, °C	–	20
Outer pressure, MPa	–	$0.1013 \times 1.2 = \mathbf{0.1216}$
<b>Forces</b> applied the end of the port	$F_{x'}$ kN	$3.706 \times 1.2 = \mathbf{4.447}$
	$F_{y'}$ kN	$-2.728 \times 1.2 = \mathbf{-3.274}$
	$F_{z'}$ kN	$2.745 \times 1.2 = \mathbf{3.294}$
<b>Moments</b> applied the end of the port	$M_{x'}$ kN*mm	$15039 \times 1.2 = \mathbf{18047}$
	$M_{y'}$ kN*mm	$-13759 \times 1.2 = \mathbf{-16511}$
	$M_{z'}$ kN*mm	$14640 \times 1.2 = \mathbf{17568}$

Forces and moments are applied to force-moment addition point called shortly FM. FM point is connected to port end nodes by MPC beam type constrain, shown in Figure 2.6.

Shell parts of vessel and PV are connected to solid center part (highlighted magenta) by shell to solid coupling type constrain, shown in Figure 2.7.

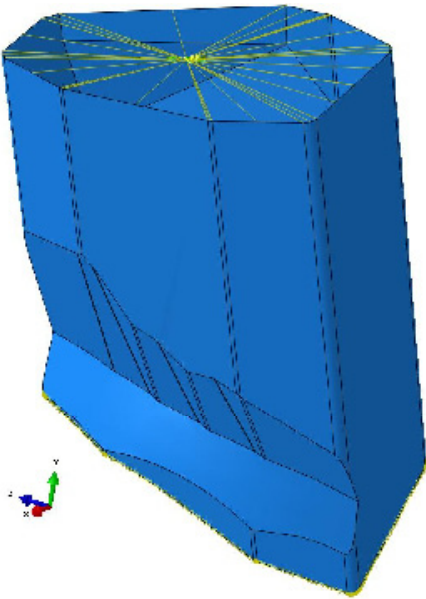


**Figure 2.6**  
FM point coupling to port

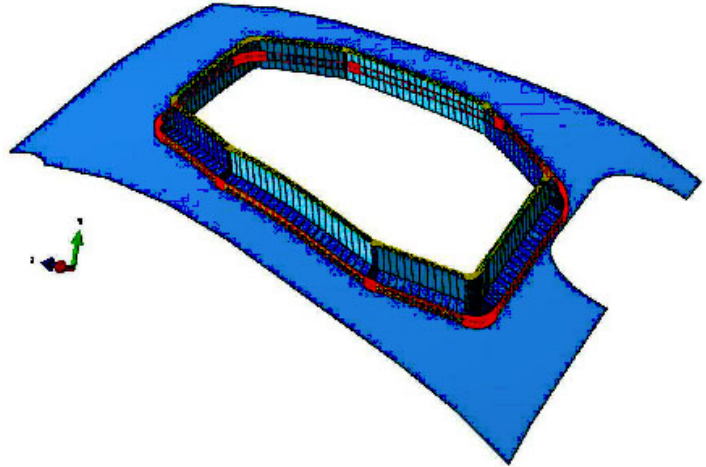


**Figure 2.7**  
Shell-to-Solid coupling

## 2.2 Results of limit load analysis for port AEK20

The limit load scaling factor analysis of the welding connection between the port AEK20 with gap 1 mm and the PV shell was performed.

The weld material for all ports was chosen as a material with ideal plastification at the level of  $1.5 \cdot s_m \cdot K_{\text{weld}}$ . Here  $K_{\text{weld}}$  is a weld efficiency factor. For these welds the values  $K_{\text{weld}} = 0.7$  and  $K_{\text{weld}} = 0.85$  was taken. The analysis results were presented at both weld efficiency factor values.

According to limit analysis results in port AEK20 with gap 1 mm in case the weld efficiency factor values 0.85 load limit SF are 6.2391 for v1 and 6.2426 for v3. In case the weld efficiency factor values 0.7 load limit SF are 5.9937 for v1 and 5.9994 for v3.

In this section the stress analysis of the welding connection between the port AEK20 and the PV shell using the weld efficiency factor value 0.85 was presented. The history of the displacement of the point where loads are applied during analysis is presented in Figure 2.8.

According to the results of the analysis, it was detected that displacement of the point where loads are applied increases linearly until scale factor  $SF = 4.5$ . The yielding of displacement will occur from  $SF = 4.5$  until  $SF = 5$ . Over  $SF = 5$  the displacement starts to increase very rapidly. The convergence of the FE analysis was lost over  $SF = 6.2426$  for version of analysis v3 and the stability of port AEK20 with gap 1 mm will be lost. According to this the limit load will be reached at loading factor of 6.2426.

Displacement magnitude distributions at end step analysis, i.e.  $SF = 6.2391$ , in this model for version of analysis v1 are presented in Figure 2.9. Maximal displacement magnitude 38.74 mm is obtained on the wall of the port.

Displacement magnitude distributions at end step analysis, i.e.  $SF = 6.2426$ , in this model for version of analysis v3 are presented in Figure 2.10. Maximal displacement magnitude 38.92 mm is obtained on the wall of the port.

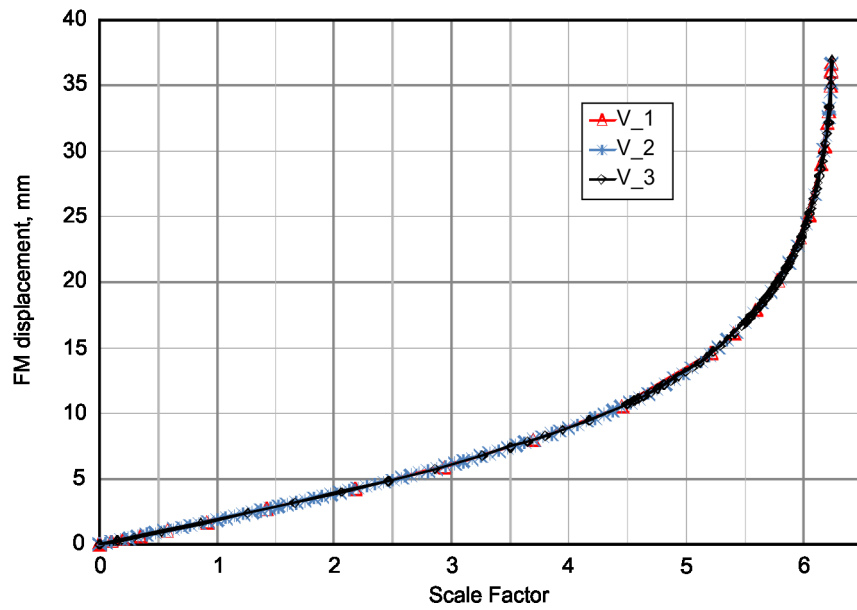


**Figure 2.8**  
Displacement of force-moment addition point

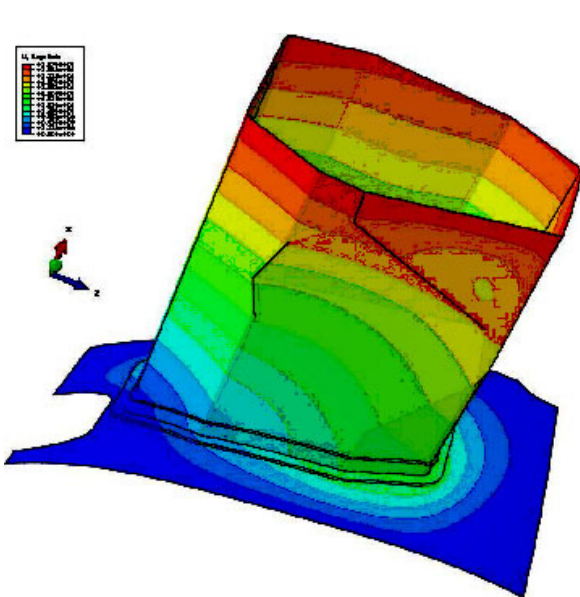


**Figure 2.9**  
Distribution of displacement in model  
AEK20 h1 k085 v1

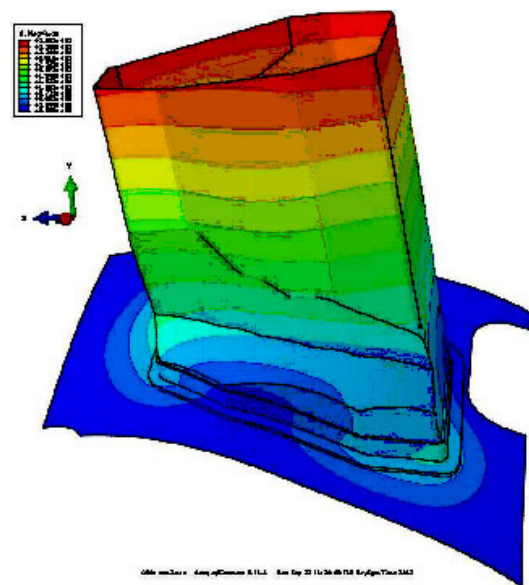


**Figure 2.10**  
Distribution of displacement in model  
AEK20 h1 k085 v3

Maximal obtained stress level is 714.9 MPa (Figure 2.11), on the weld tip. Stress distribution in cross section of weld in area of maximal stress 714.9 MPa is presented in Figure 2.12. It was received that the stresses in weld of port AEK20 and the vessel exceed the yield strength which is 320 MPa, and the stresses in the weld also exceed the yield strength which is 272 MPa.

The distribution of equivalent plastic strain at the port and PV around the weld, and the weld are presented in Figure 2.13. The equivalent plastic strain zones are located in the weld seams. It is seen that the enlarged attention should be applied in the weld tip inspection as its place of stress and strain concentrations.

According to the stress and equivalent plastic strain results it possible to maintain that failure of the port will have ductile character.

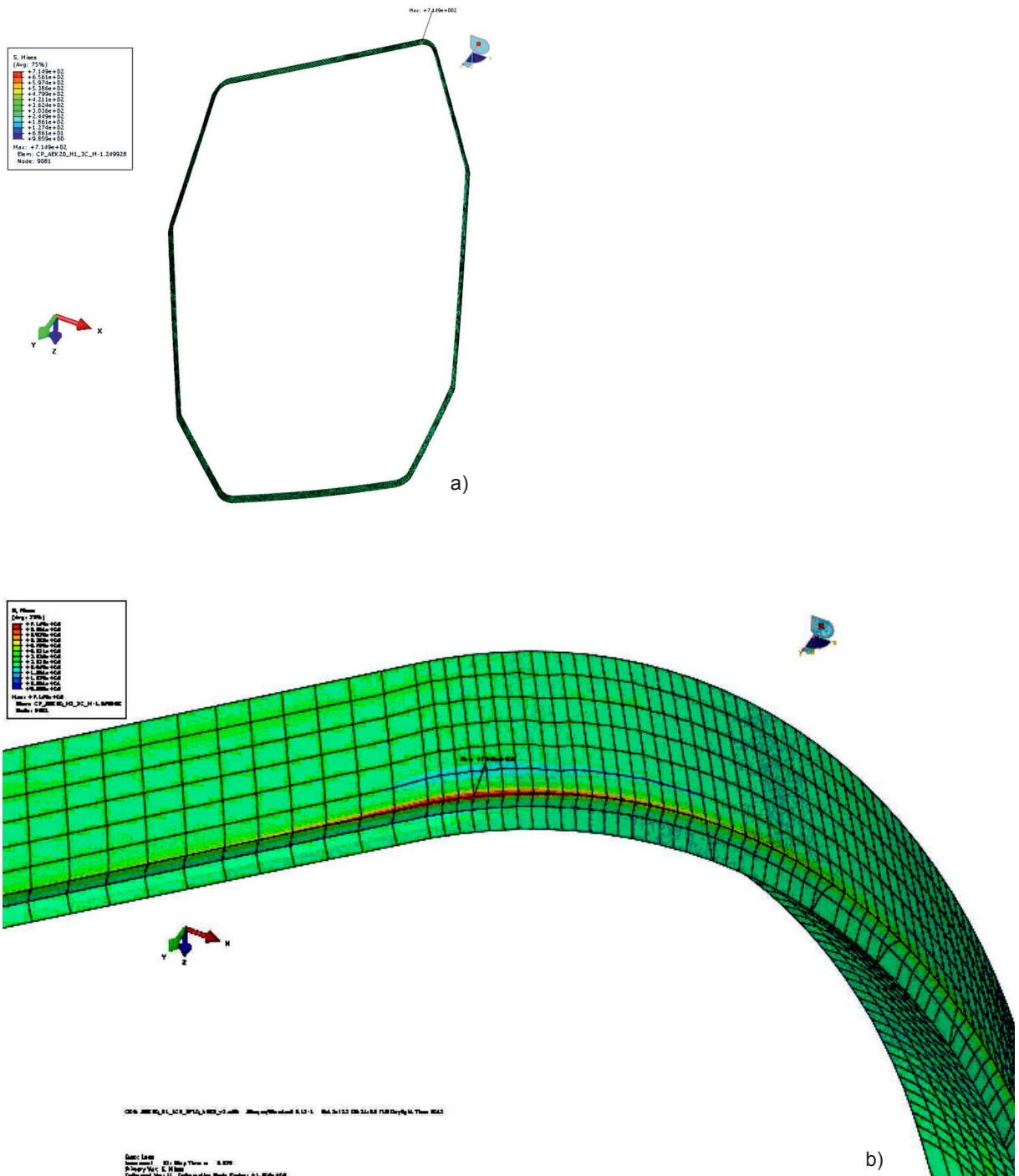


**Figure 2.11**  
Stress distribution in modelled solid weld, maximal stresses 714.9 MPa: a) – full view, b) – enlarged view around maximal stresses

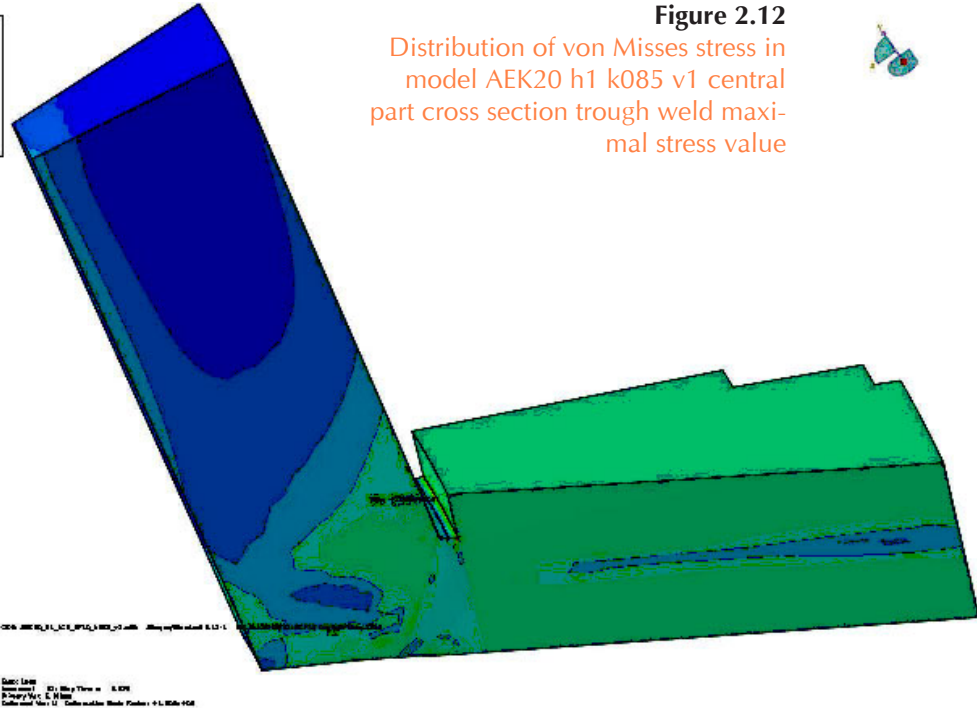
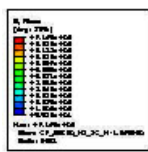


**Figure 2.12**  
Distribution of von Mises stress in model AEK20 h1 k085 v1 central part cross section trough weld maximal stress value

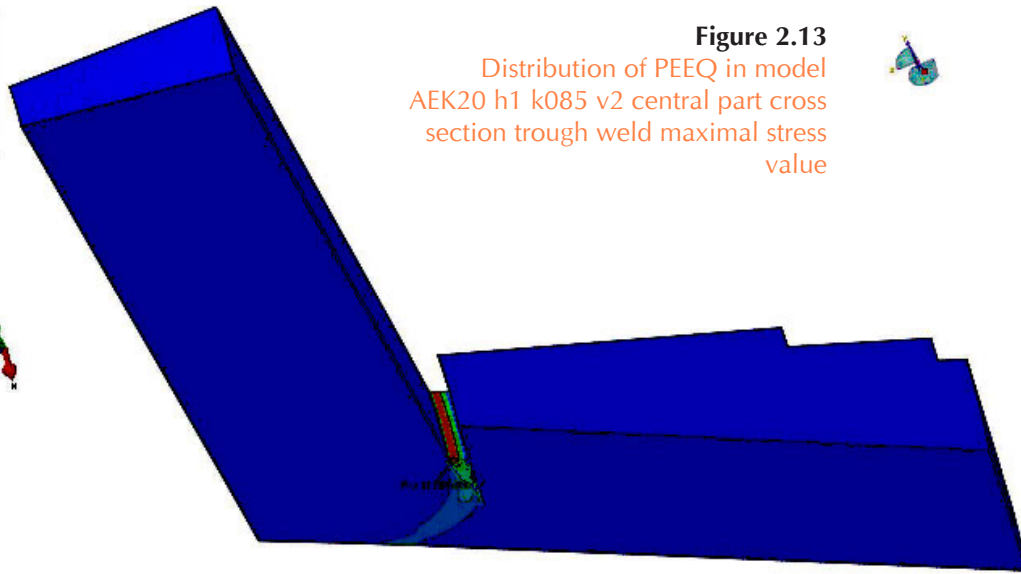
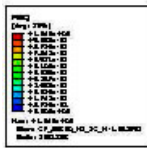


**Figure 2.13**  
Distribution of PEEQ in model AEK20 h1 k085 v2 central part cross section trough weld maximal stress value

In this section, the stress analysis of the welding connection between port AEK20 and the PV shell using the weld efficiency factor value 0.7 was presented. The history of the displacement of the point where loads are applied during analysis is presented in Figure 2.14.

According to the results of the analysis, it was detected that displacement of the point where loads are applied increases linearly until scale factor SF = 3.8. The yielding of displacement will occur from SF = 3.8 until SF = 4.5. Over SF = 4.5 the displacement starts to increase very rapidly. The convergence of the FE analysis was lost over SF = 5.9994 for version of analysis v3, and the stability of port AEK20 with gap a 1 mm gap will be lost. According to this, the limit load will be reached at loading factor of 5.9994.

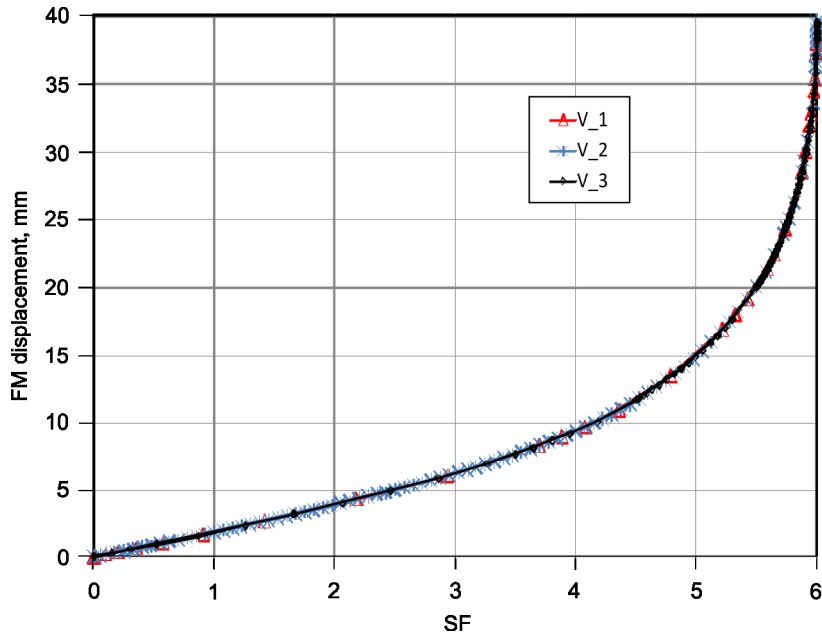


**Figure 2.14**  
Displacement of force-moment addition point

Displacement magnitude distributions at end step analysis, i.e. SF = 5.9937, in this model for version of analysis v1 are presented in Figure 2.15. Maximal displacement magnitude 39.94 mm is obtained on the wall of the port.

Displacement magnitude distributions at end step analysis, i.e. SF = 5.9994, in this model for version of analysis v3 are presented in Figure 2.16. Maximal displacement magnitude 41.57 mm is obtained on the wall of the port.

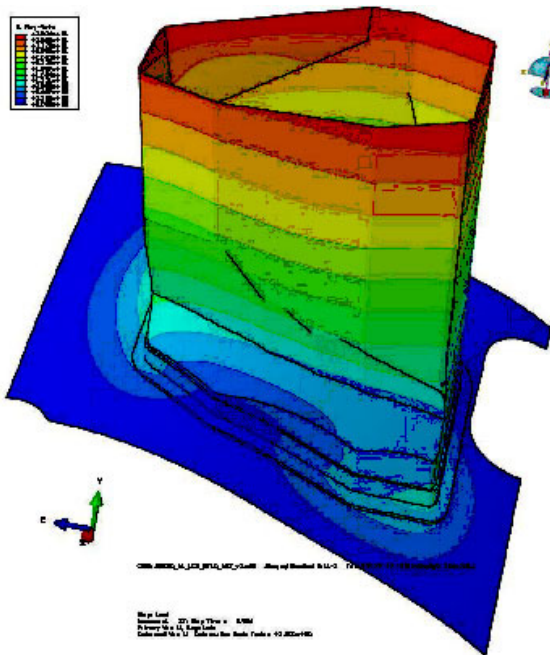


**Figure 2.15**  
Distribution of displacement in model AEK20 h1 k07 v1

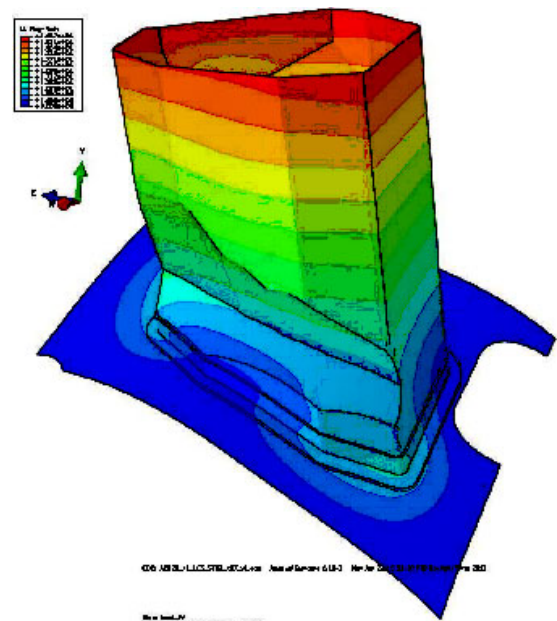


**Figure 2.16**  
Distribution of displacement in model AEK20 h1 k07 v3

Maximal obtained stress level is 661.2 MPa (Figure 2.17), on the weld tip. Stress distribution in cross section of weld in area of maximal stress 661.2 MPa is presented in Figure 2.18. It was received that the stresses in the weld of port AEK20 and the vessel exceed the yield strength, which is 320 MPa, and the stresses in the weld also exceed the yield strength, which is 272 MPa.

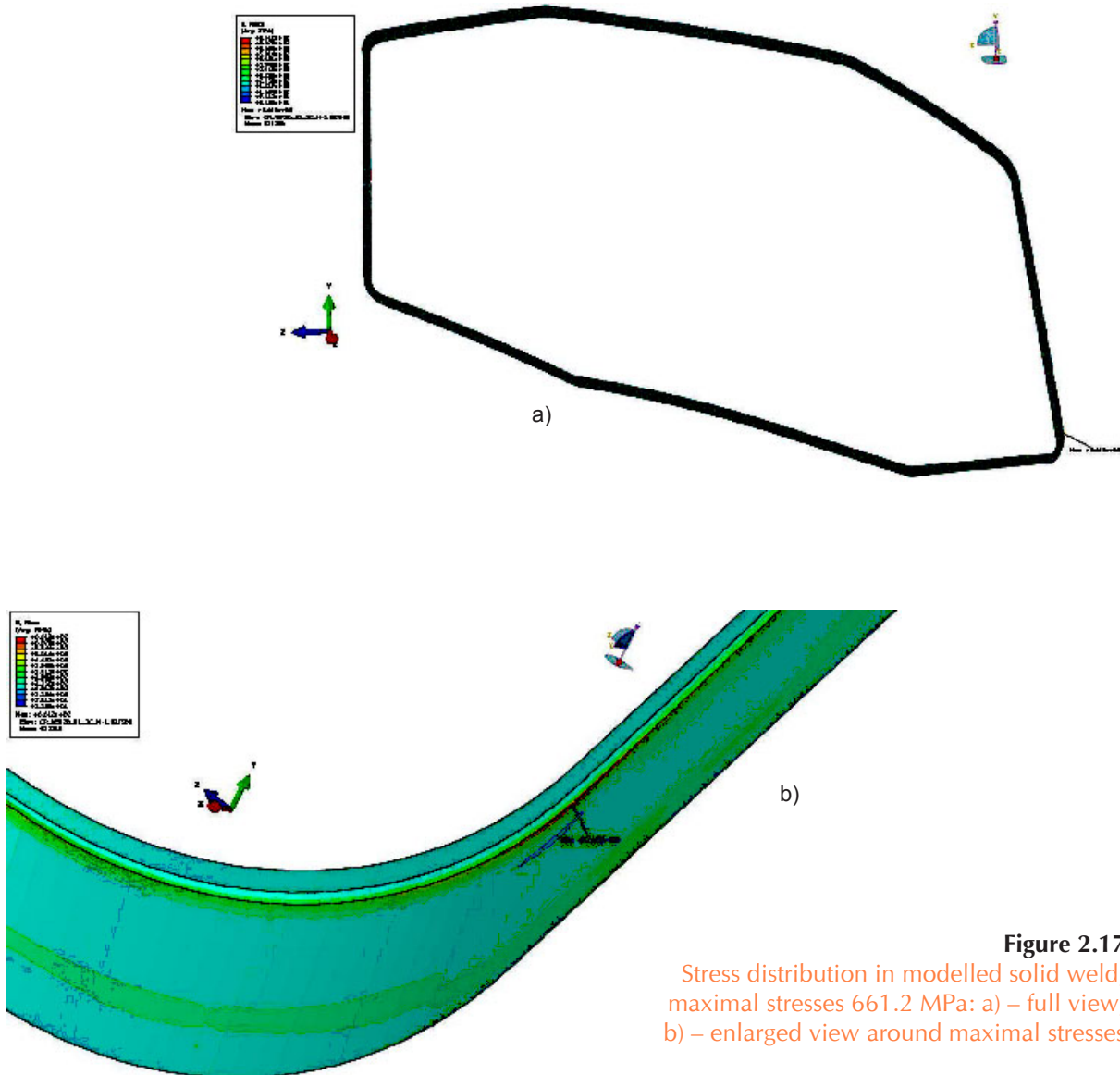


**Figure 2.17**  
Stress distribution in modelled solid weld, maximal stresses 661.2 MPa: a) – full view, b) – enlarged view around maximal stresses

The distribution of equivalent plastic strain at the port and PV around the weld, and the weld are presented in Figure 2.19. The equivalent plastic strain zones are located in the weld seams. It is shown that the special attention should be paid for inspection of the weld tip as this is a place of stress and strain concentration.

According to the stress and equivalent plastic strain results, it is possible to maintain that failure of the port will have ductile character.

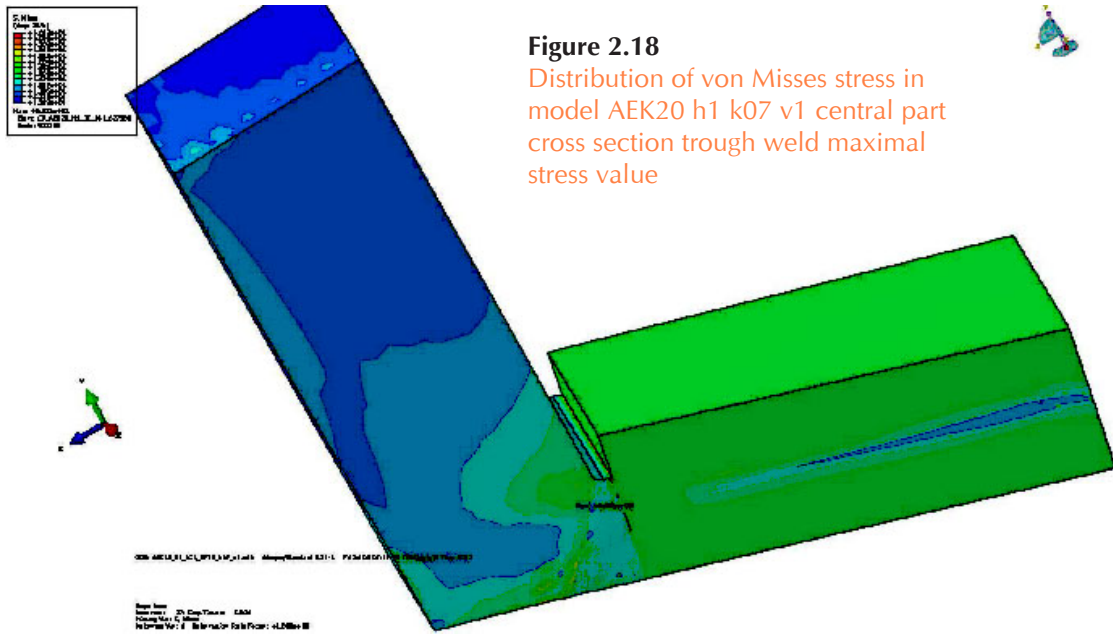


**Figure 2.18**  
Distribution of von Mises stress in model AEK20 h1 k07 v1 central part cross section trough weld maximal stress value

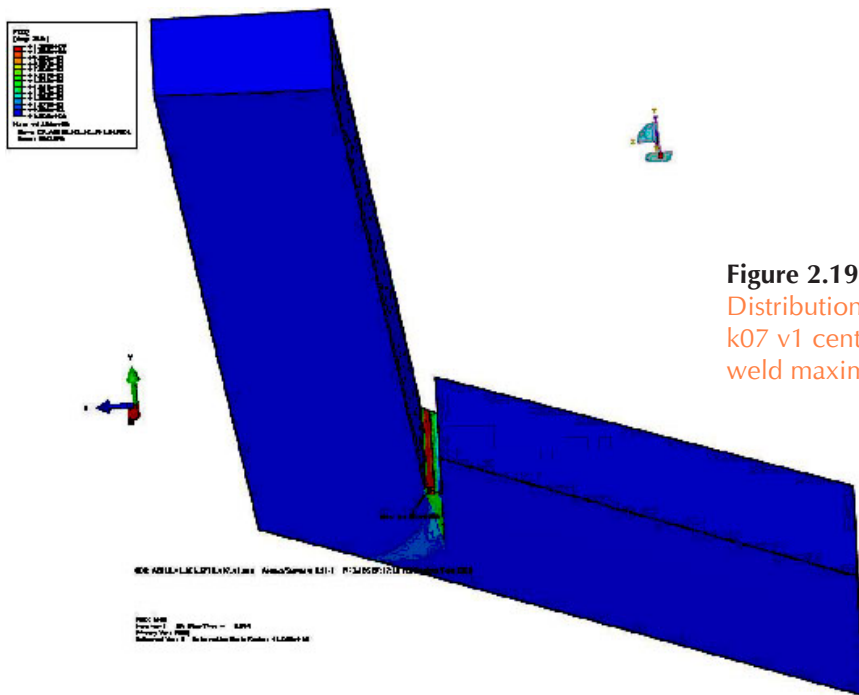


**Figure 2.19**  
Distribution of PEEQ in model AEK20 h1 k07 v1 central part cross section trough weld maximal stress value

### 2.3 Summary of the limit load analysis

The analysis of the welding connection between port AEK20 and the PV with a 1 mm gap for limit load scale factor was performed. For these welds the weld efficiency factor values  $K_{weld} = 0.7$  and  $K_{weld} = 0.85$  were used.

The final versions of histories of the displacement of the point where loads are applied for port AEK20 with a 1 mm gap are presented in Figure 2.20. From the displacement dependency presented in this figure, it is seen that decreasing weld efficiency factor values decrease limit load SF. The convergence was lost at the end of the analysis; the last calculated point is load limit SF.

The limit analysis results showed that in the port AEK20 with a 1 mm gap with weld efficiency factor values 0.85 and 0.7 the limit scale factor is 6.2 and 6.0, respectively.

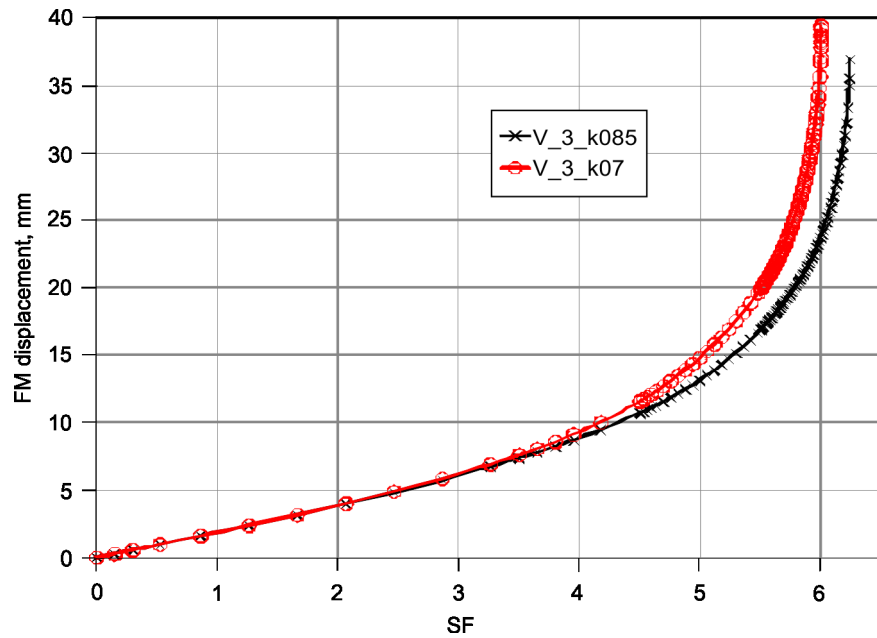


**Figure 2.20**  
 FM displacement dependency on SF in different weld efficiency factor values 0.85 and 0.7

### 3 RELIABILITY ANALYSIS OF W7-X DIVERTOR TARGET COOLING CIRCUIT AND PLASMA VESSEL AND PORTS COOLING CIRCUIT

The principal investigators for this task are R. Alzbutas and R. Voronov of LEI.

There are a number of water cooling circuits, which ensure cooling of plasma vessel components:

- Target cooling circuit ACK10;
- Baffle/Wall cooling circuit ACK20;
- Plasma vessel/ ports cooling circuit ABK10;
- Regulation coils cooling circuit ACK30/AAR10;
- ECB50.

In 2011 a pilot reliability analysis of the W7-X systems was performed in order to adopt NPP PSA experience for fusion device systems. The initial reliability analysis of a divertor target cooling circuit ACK10 and plasma vessel/ports cooling circuit ABK10 was performed in a limited scope in order to demonstrate possibilities, advantages and possible applications and gains of the analysis. The initial limited analysis included only part of possible ACK10 and ABK10 failure modes. In 2013 it was planned to continue and to refine the water cooling circuits reliability analysis in the following areas:

1. Expand the analysis scope of ACK10 including other failure modes (pipe breaks, in-vessel leakage etc.) during plasma operation and also consider baking operation mode, which can be very important for availability and safety of W7-X.
2. Perform reliability analysis of ABK10 in the same scope as ACK10 for plasma operation mode.

The performed analysis continued and finalized reliability analysis of water cooling circuits ACK10 and ABK10 performed in 2011.

The main objectives of this analysis are as follows:

1. Estimate reliability of water cooling circuits ACK10 and ABK10 for the considered operation modes;
2. Identify the main contributors (equipment failures of personnel errors) to unreliability.
3. Propose measures for reliability improvement.

In addition, the reliability analysis should provide estimation of two aspects of the water cooling circuits reliability:

- Average long-term reliability, i.e. reliability for the operating campaign (4 month) or for operating year which would include two campaigns;
- Short-term reliability analysis, i.e. ability to perform the system functions during the experiment.

The reliability analysis should include analysis of both equipment failures and human errors.

Scope of the reliability analysis should include:

- Familiarization with the systems and equipment, collection of initial data;
- Development of reliability models;
- Estimation of reliability parameters, including failure rates and repair rates for equipment and human error probabilities for personnel;
- Calculation, verification and validation of results.

The analysis results should include numerical results, including importance and sensitivity analysis, conclusions and recommendations.

Reliability analysis should be performed using specialized and verified reliability analysis software RiscSpectrum PSA legally owned by LEI.

Reliability analysis of two cooling circuits of Wendelstein 7-X water cooling system was performed, namely the reliability analysis for plasma vessel and ports cooling circuit ABK10 and divertor target cooling circuit ACK10.

The analysis was performed for baking operation mode, including baking heating and holding and baking cooling, as well as for plasma operation covering standby and plasma experiments. System structure, configurations and operation were studied, failure modes, their effects and criticality for systems operation, failure occurrence and correction possibilities were analyzed. Failure rates for different failure modes were estimated based on generic reliability data and on engineering judgement. Repair times were estimated based on IPP operation experience and engineering judgement. Pipe breaks and leakages were considered as well as failures of external systems.

Fault tree models for all considered systems and operation modes were developed. Due to high impact of pipe breaks and internal failures, two types of models were developed and analysed separately: 1) models including pipe failures and external failures and 2) "bare" models without pipe breaks and internal failures.

Unavailability of both circuits for baking operation mode, including baking heating and holding and baking cooling, as well as for plasma operation was estimated, and the main contributors to the unavailability were identified.

The following conclusions can be made:

- Due to low redundancy of equipment both circuits are vulnerable to single failures when failure and repair of one component disable the whole circuit.
- Unavailability of the cooling circuits for plasma operation is 10% for PVPCC and 12% for DTCC without consideration of pipe breaks and external failures. Additional consideration of these failures increases the unavailability up to 18.7% for PVPCC and up to 20.4% for DTCC.
- Unavailability of the cooling circuits for baking is very low due to short time of these modes. The highest (2.5%) is unavailability of DTCC for baking heating considering pipe breaks and external failures. All other unavailability estimates are not higher than 1%.
- Pipe breaks inside the plasma vessel and cryostat play very important role due to their high failure rates and long repair time. Unavailability due to pipe rupture inside the pressure vessel is higher. However, as estimations of failure rates and repair times were based on engineering judgement, these conclusions should be taken with caution.
- External failures play important role as well. For baking cooling stage loss of external power supply prevails over plasma vessel pipe break. The same as above, estimations of failure rates and repair times were based on engineering judgement, therefore these results should be taken with caution.
- When considering the "bare" circuits without pipe failures and external events, the main contributors for unavailability are the following equipment failures:

- o Heater failure for PVPCC during baking heating;
- o Failure of pumps for PVPCC baking cooling;
- o Failure to start secondary pump and failure to run primary pump for PVPCC during plasma operation;
- o Baking pump failure and heater failure for DTCC during baking heating and pump failure for baking cooling;
- o Failure to start the secondary pump, failure to open the valve on the secondary pump pressure line and failure to run the primary pump for DTCC during plasma operation.
- Pipe breaks as well as loss of cooling circuits water circulation can be initiating events for accident which may lead to serious W7-X equipment damage and, subsequently, long and expensive repairs and long unavailability for experiments.

From above listed results and findings the following recommendations regarding improvement of the cooling circuits unavailability can be made:

- Reduce unavailability of the circulating pumps ABK10 AP001, AP002 and ACK10 AP002, AP003 by either improving their reliability or by reducing their repair times;
- Consider unavailability due to pipe breaks inside the pressure vessel and cryostat due to either improvement of pipe reliability or by reducing the repair times.

The following recommendations regarding the reliability analysis can be made:

- Perform a more detailed analysis of pipe breaks inside the pressure vessel and cryostat in order to get more exact failure rates and repair times;
- Perform a more detailed analysis of external systems failures in order to get more exact failure rates and repair times;
- Perform an analysis of possible accidents and consequences of pipe breaks and loss of water circulation.

## 4 ACTIVATION CROSS SECTIONS FOR DD, DT AND TT NEUTRONS FROM JET PLASMAS

The principal investigator for this task is G. Stankūnas of LEI.

Joint European torus (JET) is presently the world's largest nuclear fusion research facility. It plays an important role in preparing the operations on the future world's largest tokamak, ITER.

In 2010 JET wall was replaced by the ITER-like wall (ILW) made of Beryllium, Tungsten and Tungsten coated on Carbon. The replacement of wall, as well as other significant modifications occurred in time, affected the neutron yield measurements, which are the basis for the determination of the absolute fusion reaction rate. Recently, a new calibration of the JET neutron detectors, including external fission chambers (KN1) and the activation system (KN2), was performed using a  $^{252}\text{Cf}$  source deployed in many toroidal and poloidal positions inside the vacuum vessel. In the coming years a new DT experimental campaign (DTE2) is planned at JET. The neutron detectors, fission chamber and activation system will have to be calibrated at 14 MeV neutron energy using a well calibrated and characterized DT neutron generator. The target accuracy for the neutron calibration is  $\pm 10\%$ .

The activation system plays an important role in the absolute calibration of neutron detectors. It relies on the measurement of the neutron induced activity in foils exposed to the neutron source, and on calculations of activation coefficients for the activation reactions used, in order to relate the local neutron flux to the neutron source intensity during calibration or plasma operation. Such calculations require an accurate knowledge of activation cross sections as the uncertainty on cross sections propagate directly in the uncertainty in the neutron yield measurements because the calibration spectrum is not equal to the plasma neutron spectrum (and whenever the reactions used during calibration are not the same used during plasma operation). Whenever possible, dosimetric reactions with well-known cross sections are used. Usually, the uncertainty in such cross section is considered negligible and, therefore, is neglected in the evaluation of the total uncertainty in the activation measurements.

However, whenever high accuracy is desired, as in the case of neutron detector calibration in JET, and later in ITER, the uncertainty on activation cross sections has to be considered. Moreover, specific applications in fusion devices may require the use of non dosimetric reactions:

1. high energy threshold activation reactions leading to the production of short lived gamma emitting nuclides are desired for plasma measurements with sufficient time resolution;
2. in calibration procedures, however, when neutron sources with limited intensity are used, high energy threshold activation reactions leading to the production of gamma emitting nuclides with longer decay times are desirable to allow longer exposure and avoid saturation of activity;
3. several activation reactions with different energy thresholds are needed to discriminate the different fusion sources (such as DT neutrons from triton burn up in DD plasmas) and features of the local neutron spectrum at irradiation positions;
4. pure TT plasma could be explored (as is the case in JET DTE2 planned for 2017) for which the spectrum of neutron emission is poorly known. The activation system could complement the spectroscopic measurements of the TT neutron spectrum provided that

suitable activation cross sections are available with energy threshold in the range of 3–14 MeV.

The goals of the present task are the following:

1. Assess and update the activation cross sections used in JET neutron diagnostics both at 2.5 and 14 MeV neutron energy in view of the DT campaign, with particular regard to the related uncertainty in typical JET neutron spectra, and
2. Investigate suitable activation cross sections for measuring the TT neutron spectrum. Assess the related uncertainty.

The activation reactions and fission reactions currently in use at JET have been considered, as well as new ones that could be used in the future in view of DTE2. Activation reactions were taken from the most recent International Reactor Dosimetry and Fusion File (IRDF) in 640 groups ENDF-6 form. IRDF is a standardized evaluated cross section library of neutron dosimetry reactions with uncertainty information that supersedes a widely used IRDF-2002 library. The IRDF contains cross section data and related decay data for 74 dosimetry reactions, and absorption data for three cover materials B, Cd and Gd used during the irradiation of some specific detectors.

Activation coefficients (reaction rates) have been calculated using the neutron flux spectra at JET vacuum vessel, both for DD and DT plasmas, in the required 640-energy group form and using cross sections available from more recent dosimetric library IRDF-v1.02. The related uncertainties for the JET neutron spectrum are evaluated as well using the covariance data available in the library and using tally specifications for producing the spectra in the 640-group structure. To this purpose, the RR\_UNC code that reads spectra, cross sections (in 640-group form) and covariances to calculate the uncertainties, have been used. These codes were provided by Andrej Trkov (IAEA).

Figure 4.1 contains JET DD, DT neutron spectra and  $^{252}\text{Cf}$  for the comparison.

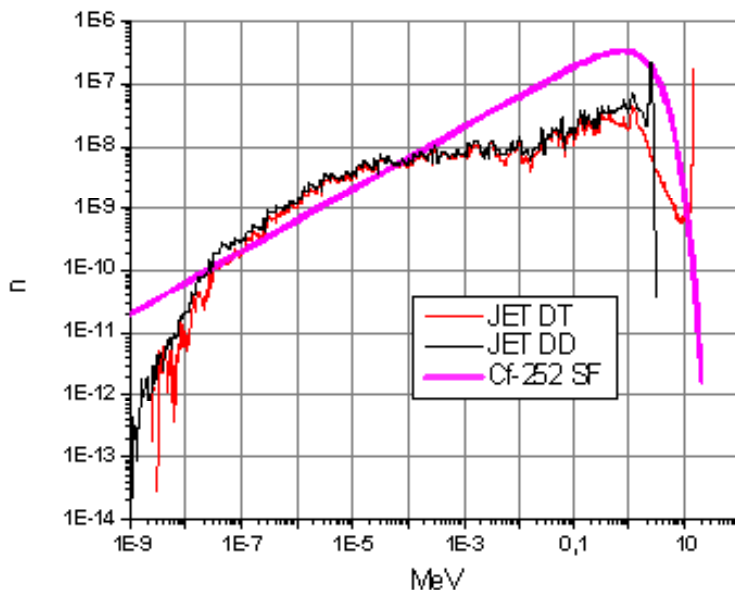


**Figure 4.1** JET DT and DD together with  $^{252}\text{Cf}$  spontaneous fission neutron spectrum

The activation reactions and fission reactions presently in use at JET have been investigated, as well as new ones that could be used in the future in view of DTE2. Activation reactions were taken from the state-of-art International Reactor Dosimetry and Fusion File (IRDFF) in 640 groups ENDF-6 form. Activation coefficients (reaction rates) have been considered using typical neutron flux spectra at JET vacuum vessel, both for DD and DT plasmas, in the required 640-energy group form and using cross sections available from more recent dosimetric library IRDFF-v1.02. The related uncertainties for the DD and DT JET neutron spectrum are evaluated as well using the covariance data available in the library and using tally specifications for producing the spectra in the 640-group structure.

## 5 ACTIVITIES IN THE FRAMES OF POWER PLANT PHYSICS AND TECHNOLOGY AGREEMENT

In 2013 LEI participated in implementation of the following tasks in the frames of Power Plant Physics and Technology Agreement:

- WP13-DTM-02: Reliability, Availability, Maintainability & Inspectability.
- WP13-SYS-02: System level analysis.
- WP13-SYS-04: Safety.

### 5.1 WP13-DTM-02: Reliability, Availability, Maintainability & Inspectability

In 2013 LEI participated in performance of two tasks regarding this topic:

- WP13-DTM-02-T02: Method to evaluate and integrate diverse RAMI input data;
- WP13-DTM-02-T04: Analysis of the DEMO Availability Requirement.

RAMI (Reliability, Availability, Maintainability, Inspectability) conception is planned to be applied for DEMO in all stages of project development. Therefore, at first the objective was to define what is initial DEMO availability and growth of availability based available historical data.

#### 5.1.1 WP13-DTM-02-T02: Method to evaluate and integrate diverse RAMI input data

The principal investigators for this task are R. Alzbutas and T. Iešmantas of LEI.

In order to make RAMI inferences for DEMO plant as accurate as possible the amount of statistical information is of crucial importance. The more data we have, the better analysis results can be obtained. However, since DEMO plant is a first of its kind, there are no statistical data available. One of possible ways out of this situation is to analyse RAMI data collected at other power plants, at similar systems that will be used in DEMO. In addition, the experience of experts cannot be ignored – elicitation of subjective opinion should be carried out and analysed together with statistical information (if available). Hence, we can see four points of RAMI inference for DEMO:

1. Assessment of available statistical information contained in various databases;
2. Elicitation of prior subjective information;
3. Joint analysis of objective (statistical data) and subjective information;
4. Posterior analysis.

The necessity of such methodology were concluded from the analysis of various reliability data sources, like WASH, lambda-predict, IAEA, T-Book, TKI, etc. Inconsistencies in records information, varying level of mathematical assumption justifications, non-existent data for DEMO, different experiences of experts – these aspects hinders the entire RAMI assessment process for the DEMO plant. Classical statistical methods do not give a hand here – this class of methods simply does not suit for such differences in information.

Hence, we proposed a methodology built entirely on Bayesian statistical notions. It enabled to create a scheme of workflow, by which those different information sources can be easily integrated into one analysis. In such way, the methodology is able to extract much more information for the sake of RAMI assessment as compared to classical tools.

On the other hand, there are some issues that need to be resolved. Like the difficulty in obtaining prior distributions based on expert opinion elicitation. There are some mathematical notions at work, which might put off practitioners from applying Bayesian methods. However, it is possible to provide some worked out examples of most common cases, so that one would not have to perform mathematical calculations (e.g. marginalization) by itself.

We demonstrated proposed methodology for a real case on HCBP water cooling cycle pipelines. By extracting additional information from databases we were able to improve posterior inferences. Out of 10 records, 5 had additional information about the probability distributions supposedly generating failure rates. This information was expressed in terms of quantiles. We assumed that this information was provided by virtual experts and out of this information prior distribution was formed.

Posterior results showed that the influence of this additional information translated into almost ten-fold differences in pipeline failure probability as compared to non-informative prior distribution.

### 5.1.2 WP13-DTM-02-T04: Analysis of the DEMO Availability Requirement

The principal investigators for this task are R. Alzbutas and T. Iešmantas of LEI.

This report aims to present analysis of the DEMO (DEMOstration Power Plant) Availability Requirement. This is partially related to the overview of previous activities in WP12, namely, “Expected initial availability and availability growth of the DEMO plant based on historical data”).

According to the EFDA glossary, DEMO is the successor of the international fusion experiment ITER (International Thermonuclear Experimental Reactor) and the next step on the way to realise fusion energy. Its purpose is to develop and test technologies, physics regimes and control routines for operating a fusion reactor not as a scientific experiment, but as a power plant. One of the key criteria for DEMO is the reliable production of electricity to the grid.

Currently no conceptual design exists for DEMO; however, in order to facilitate the work in the WP12/WP13 activities, various assumptions are made about the overall plant architecture, operational and maintenance concepts. These assumptions will be validated through the pre-concept / concept design phase of DEMO reactor that will be capable of construction in the 2030s.

The top-level requirements for this DEMO reactor are as follows:

- To demonstrate a workable solution for all physics and technology questions associated with capturing the energy released by burning plasma and converting it to a useful power flow in a safe, reliable, and sustainable manner through the successful integration of many systems and physical processes.
- To demonstrate significant net (~ several hundreds of MW) electricity production with self-sufficient tritium fuel supply.
- To achieve satisfactory availability targets.

Availability is a primary measure of effectiveness for an attractive fusion power plant and will directly affect the cost of generated electricity [7]. Two of the most important quantities that influence the availability of a fusion device are Reliability (represented by the mean time between failures, MTBF) and Maintainability (represented by the mean time to repair, MTTR).

According to the Design Tools and Methodologies Work Program 2013, LEI (Lithuanian Energy Institute) is taking part on the DTM02: Reliability Growth and Risk Minimisation of in Vessel

Components. LEI together with CCFE and VTT were in charge of developing “T04: Analysis of the DEMO Availability Requirement”.

This mission realisation from LEI side was broken into the following steps:

1. Identification of relevant measures and suitable parameters of Availability Requirement to reflect the actual efficiency (including economic output) of the DEMO facility.
2. Demonstration/modelling and clarification of various definitions and alternatives considering different measures and parameters of Availability Requirement for DEMO.
3. Analysis of selected DEMO Availability Requirement taking into account energy sector industry practice and further investigation of DEMO specific pulse-operation scheme.

DEMO availability requirement was analysed in the context of the background discussion, previous investigations and taking similar energy sector industry practice into account.

To be competitive, the final goal for FPP should have high availability, preferably exceeding 80%, with very few unplanned shutdowns. To profit from economies of scale, the plants should be large (around 1600 MW). Total construction time should be less than 5 years.

Going to this goal and knowing the historical availability of other fusion devices (mainly research installations) DEMO should meet at least 30 % availability if DEMO is more related to the research activities. In case DEMO represents the first commercial power plant, then high availabilities must be demonstrated by DEMO, and then the availability should be in the interval between 40% and 70%.

Due to various performance indicators applied in the energy industry, different availability related indicators were considered. In terms of assessing the availability requirement for DEMO: Equivalent Availability and Actual Operational Time, Operating Efficiency and Time Utilization as well as System Effectiveness and Energy Utilization are suitable parameters (performance indicators) that should be included in the modelling effort since they quantify the actual output of the facility, rather than the duration that DEMO is available to operate at some undefined capability level.

In addition, the pulse-operation model is developed to reflect a set of typical operational regimes at a macro-scale. This is related to the modified model of stand-by system, which is not used periodically, like DEMO during dwell phase. The application of this general model for DEMO purposes could be investigated in future, when more precise information regarding the DEMO will be available. This model could be extended for the economical analysis and optimisation (i.e. cost-benefit analysis) purposes.

However, only availability and market driven requirements do not include safety/security considerations. In the context of unavailability analysis (including root causes) to guarantee continued effectiveness and safety of operation during plant lifetime of DEMO, the optimisation of in-service-inspection and maintenance timing of a fusion power plant should be taken into consideration during the design of the systems.

## 5.2 WP13-SYS-02: System level analysis

The principal investigator for this task is G. Stankūnas of LEI.

Ferritic–martensitic (F–M) steels, as the structural materials, are very important for use in advanced fusion nuclear reactors. Alloying composition adjustment by computational thermodynamics and thermomechanical treatment were used to improve high strength HT F-M steels.

Enhancing energy efficiency is one of the possible ways to meet the growing energy need. To increase thermal efficiency of the advanced nuclear reactors, more aggressive environments (e.g., coolants at higher temperatures and/or pressures) have been proposed. The application of such environments needs materials with improved performance to ensure the safety margins, design

flexibility, and economics of the reactors. F-M steels are an important category of structural materials proposed for advanced nuclear reactors because of their high resistance to radiation-induced void swelling (e.g., ~1 vol.% per 100 displacement-per-atom (dpa) in F-M steels versus per 10 dpa in austenitic stainless steel at temperatures above 300 °C), high thermal conductivity, and low thermal expansion coefficients compared to SS316L(N).

Even if the fusion scientific community may be already convinced that the austenitic steel SS316L(N) is not an option for DEMO, it might be worthwhile to have a record of the consequent radioactive waste. This assessment will serve as a reference of the activity inventories to be expected in case of blanket and/or divertor were made of SS316L(N).

One of the aims of this task is to provide a comparative analysis of two types of steels, i.e austenitic steel SS316L(N) and High Temperature Ferritic-martensitic (HT F-M) steels, for computing the activation and decay heat of the central outboard blanket module.

For simplicity of the calculations, as it was agreed in the Interim meeting of the task, the comparison would be limited to the central outboard blanket module. Based on the provided MCNP model, cell 725 (or #5 mitplane down) – the full blanket segment was taken for the calculation reference.

In this section, the results obtained by the LEI in the frame of the WP13-SYS02-T08 task are showed. The task of LEI has been to obtain activity and decay heat of the central blanket (see Figure 5.1) module for the HCLL model using Eurofer as structural material and perform the benchmark for F-M steel and SS316 type stainless steel. The irradiation scenario is presented in Figure 5.2. Coupled approach for MCNP5v1.6 transport and FISPACT/EAF-2010 was used for activation calculations HCLL DEMO, where HT FM steel and SS-316L(N) were set as structural material. Calculations performed: activity inventories (Bq/kg) in structural material at 1h, 1d, 1w, 1m, 1y, 10y, 100y,

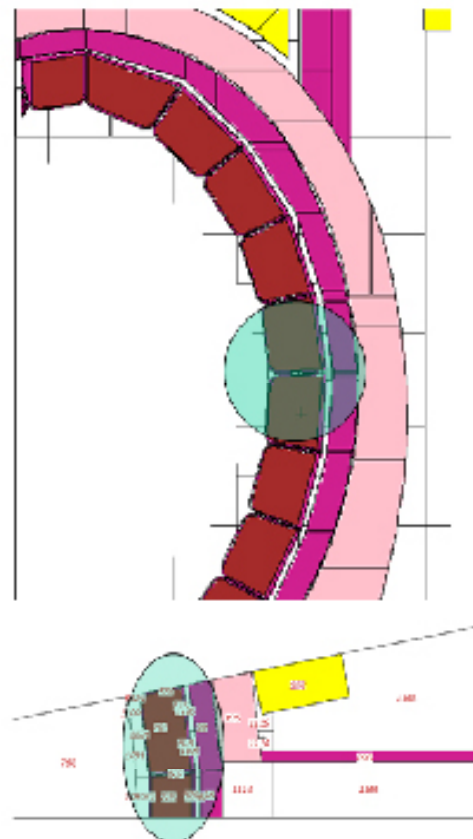


**Figure 5.1**  
Model used: filed-in the empty boxes with the HCLL material mixture

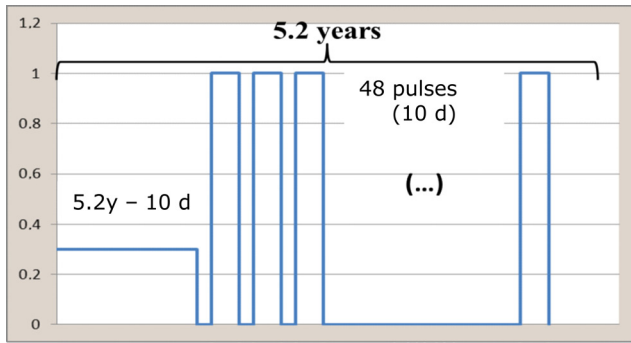


**Figure 5.2**  
Irradiation scenario

1000y after shut-down; decay heat production in central outboard blanket module at 1h, 1d, 1w, 1m, 1y, 10y, 100y, 1000y after shut-down. The after shutdown times of interest fixed for this task are 1 hour, 1 day, 1 week, 1 month, 1 year, 10 years, 100 years and 1000 years.

For this reason the complete analysis was performed by means of MCNP using JEFF 3.1.2 nuclear data library coupled with FISPACT. The statistical error of Monte Carlo calculation is about 0.1% with  $10^9$  particles histories. The calculated neutron flux in the central outboard blanket module (filed-in the empty boxes the HCLL homogeneous breeder material mixture LiPb: 85%, void 7% and structural material 8%, where SS316L(N) and HT-FM were used) was employed in FISPACT to produce activation and decay heat results. Material composition of the considered steels was used for MCNP and FISPACT calculations.

The provided strategy allowed us to obtain results for benchmark of the structural materials. In addition, Eurofer was considered as well using two different program codes, namely ACAB (done by UNED) and FISPACT (done by LEI), to have a full picture of all considered types of steels in this task. Note, that only total values of activity and decay heat are provided for Eurofer, while detailed analysis with identification of dominant nuclides were performed for SS316L(N) and HT F-M.

As we can see from the Figure 5.3, the activity for SS316L(N) is different for the longer cooling time, i.e. after 100 years, the difference can be higher by two orders of magnitude for SS316L(N), while the decrease of the activity for HT F-M and Eurofer stays the same for the entire period of cooling time.

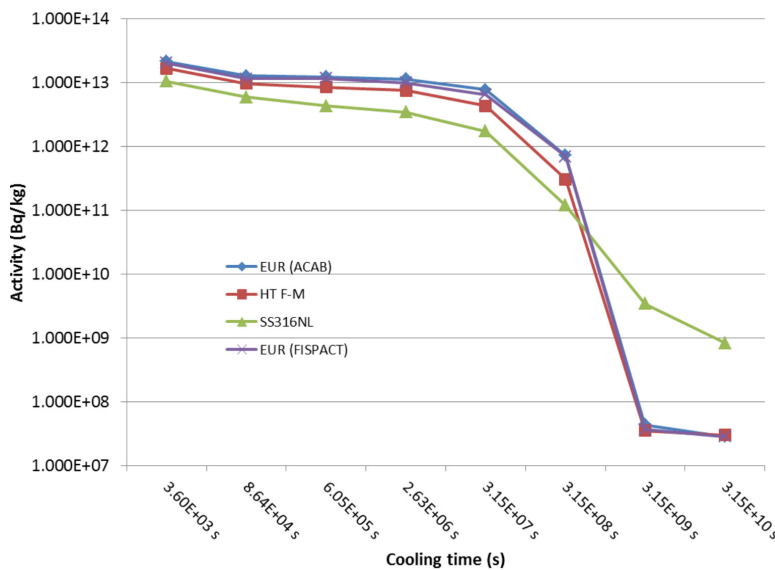


**Figure 5.3**  
Activity for investigated type of steels

The main contributing nuclide in short cooling time is mainly Mn-56, but it decays rapidly ( $T_{1/2} = 2.58$  h) and Fe-55 starts to dominate up to 10 years after the irradiation. For the longer cooling time, Ni-63 and Mo-93 became most dominating nuclides (see Figure 5.4 for details).

All three types of steels, Figure 5.5, have shown the same trend on decrease of the decay heat; however, results from ACAB on Eurofer differ from FISPACT and give higher values by up to 15%. For the SS316L(N) and HT F-M cases, we have similar situation as for activity results, i.e. HT F-M produces less heat at the end on investigated period of time.

Dominating nuclide Mn-56 is common for both types of steels, just after the stop of the irradiation, but it decays rapidly and Mn-54 takes the most dominating nuclide place. However, Ta-182 and Fe-55 plays important role in HT F-M steel, while Co-58 and Co-60 produce biggest part of the total decay heat in SS-316L(N) steel. At the end of cooling time, C-14 and Nb-93m together with Ni-63 are the most dominant nuclides for HT F-M and SS316L(N) respectively(see Figure 5.6 for details).

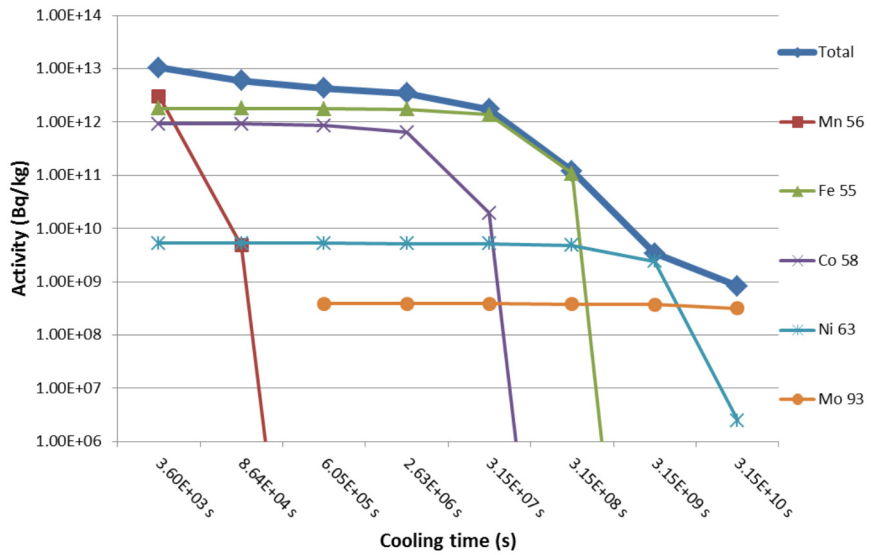


**Figure 5.4**  
Activity and dominating nuclides in SS316L(N) of the central blanket module

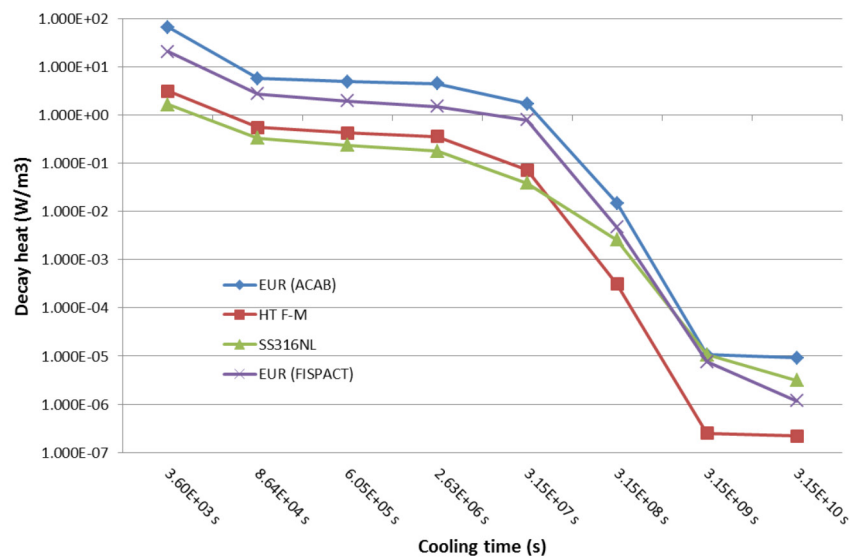


**Figure 5.5**  
Decay heat for investigated type of steels

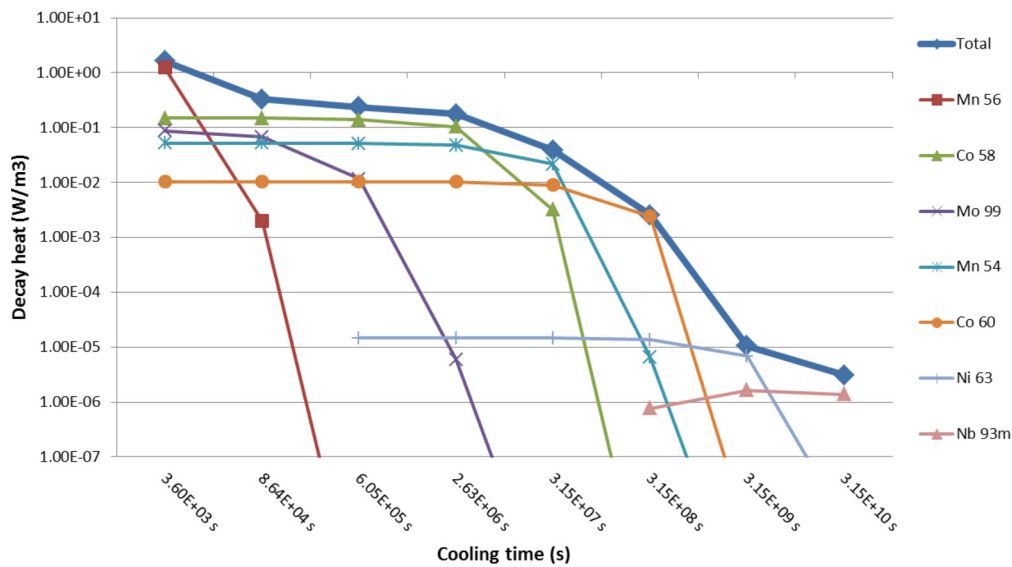


**Figure 5.6**  
Decay heat and dominating nuclides in SS316L(N) of the central blanket module

### 5.3 WP13-SYS-04: Safety

The principal investigators for this task are E. Urbonavičius and T. Kaliatka of LEI.

Task Agreement WP13-SYS-04-T05 “Review of modelling codes and identifications of development needs” was implemented together with ENEA and Rome University La Sapienza.

Safety relevant computer codes are used to model and evaluate plant conditions from normal operation up to largest credible accident situation. Several models and safety oriented codes have been developed for the licensing of more than 400 NPPs throughout the world. These models and codes have been validated or qualified for the conditions prevailing in the fission plants in various situations. Nevertheless, in fusion reactors there are present specific aspects compared to fission (the high flux of highly energetic neutrons, leading to high activation rate, the presence of rather large amount of tritium and dust, the use of specific materials). On the other hand, it can be noted that there is very little fuel inside the reactor at any time, there is low decay heat to take into account, and there are no long lived radionuclides in the ashes of the reaction.

The specific aspects and the typical temperature ranges of the plants, the potential use of specific cooling fluids, the use of other types of materials, the presence of high magnetic fields, etc. led to the need of developing specific codes and models adapted to the conditions of fusion plants.

These newly developed or extended computer codes have to be validated by conducting representative experiments or by cross checking various codes based on different modelling approaches.

The process of licensing NPPs involves the production of a comprehensive safety analysis report. The main goal being to demonstrate the safe behaviour of the concerned machine and the limited impact on the population and environment in all the operational and accident scenarios, in particular that no evacuation criterion is met. For doing it some modelling and sometimes complex calculations are needed.

A systematic safety analysis of the plant has to be carried out in order to demonstrate that the impact on public and workers is below the safety design target. The safety analysis is developed through:

- assessment of radioactive source terms and energies;
- impact during normal operation;
- radioactive releases and relevant doses following the dominant accident sequences identified through a systematic approach (like FMEA);
- radioactive waste quantification and characterization.

In order to perform the above safety analysis, dedicated computer codes have been developed through the years or adapted from existing ones, mainly coming from fission NPPs studies. All the codes have been also validated or are under validation considering the specificity of fusion plants.

To simulate accident sequences it is necessary to quantify the source terms as activation, tritium generation, activated corrosion products and dust. All these parameters can be calculated during the accident simulation or before with other tools and used as inputs. The first option is complex because it requests the coupling of computer codes different in models and architecture. The second option is preferred. For this reason the codes for the source term evaluation can be considered as design tools. In fact they are necessary to quantify activation, tritium, activated corrosion products and dusts production in normal operating conditions. Due to that they are not included in the list of the code this report deals with.

A brief overview of the most relevant code used for accident analysis in fusion reactors is introduced below.

MELCOR was originally developed at Sandia National Laboratory as a fully integrated code that models the progression of severe accidents in LWRs. MELCOR can analyze the severe accidents that involved thermal hydraulic response of the primary reactor coolant system, the confinement buildings, the reactor cavity, the containment, in-vessel and ex-vessel hydrogen production, transport, and combustion, heat structure response. A version for fusion reactor was developed at Idaho National Laboratory and it was support for fusion applications as ESECS, NSSR-1, NSSR-2 and GSSR.

CATHARE code (developed by IRSN, CEA, AREVA and EDF) simulates a two-phase thermal-hydraulic circuit of LWR, in particular, in PWR. CATHARE for fusion applications was used since 2005 to simulate the divertor circuit and the possible accidents that involve this one and the primary circuit. Very few tests were performed with the use of the COMSOL Multiphysics code (COMSOL Group) in these last years in the fusion context. Korean studies start to approach the use of COMSOL for the safety of nuclear fusion reactor. Other studies were performed at ENEA-FUS in Frascati (Italy), by using STARDUST experimental facility.

The CONSEN code (University of Rome "Sapienza" and ENEA) is a fast running program suited to simulate thermal hydraulics transients in the interconnected volumes affected by an accident, with particular reference to cryogenic conditions. The CONSEN code was used in the past for several accident analyses related to ITER.

The numerical code system MAGS was set up in 1995 at the Institute of Reactor Safety of the Forschungszentrum Karlsruhe (now Karlsruhe Institute of Technology), to analyze the 3D quench behavior of superconducting forced flow cooled magnet coils of cable in conduit conductor type (CICC) as used for Tokamak fusion applications. In this way, complex accident scenarios with interacting effects can be treated by MAGS.

AINA is a computer code that integrates a global balance plasma dynamics model and a radial and poloidal thermal analysis of in-vessel components, developed by FEEL/UPC/Barcelona-Tech. The code calculates the initial equilibrium to match one of the ITER reference scenarios and then, calculates the transient evolution for the configured perturbations, which can affect a portion of the blanket modules (LOCA), the plasma (Loss of Plasma Control Transients) or can damage a portion of the blanket modules causing a loss of coolant accident (LOCA). The two abnormal events can occur and be simulated at the same time, too.

CHEMCON was developed by INL to analyze thermal transients in order to simulate temperature excursions in the first wall and blanket components during LOFA and LOVA scenarios. In ITER CHEMCON was used to simulate the transient thermal hydraulics with 1-D scoping tool INTRA (from JED Gmbh and STUDEVNIK NUCLEAR) has been used during 1996-2006 for the analyses of accidents in Tokomaks.

INTRA is a general containment systems code, based on lumped-parameter technique, handling thermal-hydraulic behaviour in buildings and vessels, chemical reactions and distribution of non-condensable gases. INTRA code was one of the main codes applied for ITER accident analyses from the beginning of the safety assessment of the plant for LOCA and LOFA events.

The SIMMER-code family, developed at Los Alamos National Laboratory, has played an outstanding role in the framework of safety code development for LMFBRs (90's years); it is applied also in fusion safety studies since the beginning of this century. The entire code consists of three elements: the fluid dynamics model, the structure model, and the neutronics model.

GASFLOW code was developed by LANL, DOE and NRC in USA. Recently it is supported and applied to the nuclear fusion context by the Institute for Nuclear and Energy Technologies at KIT. It is a CFD code used as a best-estimate tool for predicting transport, mixing, and combustion of hydrogen and other gases in nuclear reactor containments and other facility buildings.

TRAC is an advanced "best-estimate" computer code, developed for analyzing transients in thermal-hydraulic systems. Specifically, TRAC-PF1/MOD1 was developed for analyzing postulated accidents in PWRs. It was modified at JAEA and used for simulation of thermal-hydraulic transients at abnormal conditions in fusion reactors, about a decade ago.

ANSYS FLUENT is a state-of-the-art computer program for modelling fluid flow, heat transfer, and chemical reactions in complex geometries. ANSYS FLUENT is suited for incompressible and compressible fluid-flow simulations. In the fusion context the ANSYS (thermal analysis code) was applied several times (last years) in the safety assessment relating to the TBM for the accident analyses of HCPB concept.

ASTEC is a code system developed by IRSN and GRS to compute severe accident scenarios and their consequences in Pressurised Water Reactors. Its capabilities have been recently extended, in these last years, to address the main accident sequences which may occur in the fusion installations, in particular in ITER This first fusion version of the ASTEC code has been developed with the objective to be able to perform the analyses of a LOVA and a LOCA.

RELAP5/MOD3.3 has been developed jointly by the NRC and a consortium consisting of several countries and domestic organizations that were members of the International Code Assessment and Applications Program (ICAP). The mission of the program was to develop a code version suitable for the analysis of all transients and postulated accidents in Light Water Reactor systems, including both large- and small-break LOCAs as well as the full range of operational transients.

The ATHENA (Advanced Thermal Hydraulic Energy Network Analyzer) code was developed at the Idaho National Laboratory as part of a DOE program for use in investigating safety issues associated with fusion power systems. ATHENA was designed with a structure similar to the RELAP5.

The RELAP/SCDAPSIM code, designed to predict the behaviour of reactor systems during normal and accident conditions, is being developed as part of the international SCDAP Development and Training Program (SDTP). The code version, MOD3.4, is also used for general user training and for the design and analysis of severe accident related experiments. RELAP/SCDAPSIM/MOD4 is the latest experimental version available only to SDTP members and it is the first version of RELAP5 that has been completely rewritten to FORTRAN 90/95 standards.

The RELAP5-3D code is an outgrowth of the one-dimensional RELAP5/MOD3 code developed at the Idaho National Laboratory (INL) for the U.S. Nuclear Regulatory Commission (NRC). The application of RELAP5 to these various reactor designs created the need for a 3D flow model. The newest version to be released in October 2013 is RELAP5-3D Version 4.1.3.

The Containment COde SYStem (COCOSYS) provides a code system on the basis of mechanistic models for the comprehensive simulation of all relevant processes and plant states during severe accidents in the containments of Light Water Reactors, also covering the design basis accidents.

FUS-TPC is a new simplified fusion-devoted version of the fast-fission one called SFR-TPC developed to study tritium inventories and losses from Sodium-Cooled Fast Reactors. The code has been firstly developed in 2011 to analyze tritium transport in the European configuration of the HCLL blanket for DEMO.

ECOSIMPRO is a multidisciplinary simulation tool that belongs to Empresarios Agrupados (EA) and it has been developed by EA under partial European Space Agency funding. The code and its TRITIUM\_LIBS libraries are now being used in a new area in order to model the European Test Blanket System.

At the end of the survey the criteria followed for the code selection were to keep:

- two codes facing peculiar DEMO problems for validation and QA reasons. Therefore the two codes specific for the analysis of the tritium transport and permeation, FUS-TPC and ECOSIMPRO, have been put in the list. To simulate the liquid metal in the breeder box in HCLL and in WCLL the codes SIMMER and RELAP5-3D seemed the most suitable then they are included;
- all the codes dealing with events not covered by other codes, like AINA for plasma transients, MAGS for magnet events and GASFLOW for detonation/deflagration;
- the higher ranked CFD code to study the localized phenomena, that is ANSYS-FLUENT;
- two codes covering the whole transient from thermal-hydraulic to the release, that are MELCOR and ASTEC, always for validation and QA issues;
- the higher ranked among the pure thermal-hydraulic codes, RELAP5/MOD3.3;
- one fast running code for scoping studies, CONSEN.

Figure 5.7 shows the proposed selection.

A set of computer codes suitable for the DEMO accident analyses has been scrutinized and selected. It can cover reasonably the most part of the accidents occurring in DEMO reactor, with some lacunas due to missing models and missing comprehension of physical peculiar phenomena.

A structured program of QA should be planned or the future to have in fusion, as in the fission context, a set of reliable codes. The documentation should be homogeneously structured to trace the code evolution and the tests performed.

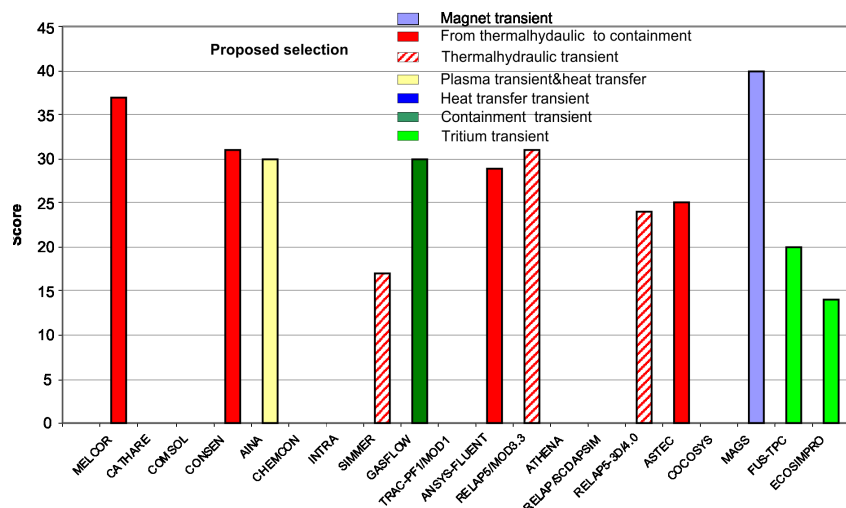


Figure 5.7 Selected computer codes

The uncertainties evaluations should be one of the key points in the code choice and it is currently one of those disregarded. How to face this issue could be a serious challenge for the future DEMO project.

The list of the most critical models to be implemented in the codes to fit all the phenomena necessary for DEMO accident simulations has been inferred.

To support the modelling, experiments should be planned to cover some critical issues that are not included in the current version of the simulation codes, such as the chemical reactivity of the beryllium pebble bed and dust taking care of:

- the extension of the range of application of the existing data, because the reaction rate correlation for Be-steam reaction are valid in a certain range of temperatures only;
- the influence of the pebble density and dimension, because the experimental evidences do not give clear indications about the chemical reactivity if compared to dense beryllium;
- the heat transfer in the HCPB pebble beds because it plays a significant role in the accident evolution.
- the Be dust inventory mobilizable from HCPB TBM box that is an unknown parameter.

Other basic experiments necessary for code validation are those on the chemical reactivity of the LiPb with air and steam. This reaction has to be investigated extensively in a wide range of cases covering the DEMO events experiments and those relating to the formation of ACPs in LiPb circuit under irradiation and the modelling implemented in the selected codes.

The selection that has been done is not conclusive in the frame of PPP&T programme, but it is referring to the current status of the code development.

Being the DEMO PPP&T work-programme a living project for the next years, the choice of the codes could change, according to the safety study needs and the code evolution.

## 6 CALCULATIONS OF SPECTROSCOPIC CHARACTERISTICS FOR W IONS

Principal investigators in this task are P. Bogdanovich, G. Gaigalas and A. Kupliauskienė of VU ITPA.

### 6.1 Investigation of the $4p^64d^N \rightarrow 4p^64d^{N-1}4f + 4p^54d^{N+1}$ excitation of highly charged $W^{+37}$ , $W^{+36}$ and $W^{+35}$ tungsten ions by electrons within Born approximation in quasi-relativistic approach with the correlation effects included

The developed quasi-relativistic approach for the calculation of the energy spectra and radiative transition probabilities was adopted for the calculation of collision strengths, excitation rates and excitation cross sections for the excitation by electron impact of the  $W^{+37}$ ,  $W^{+36}$  and  $W^{+35}$  ions. We have solved the quasi-relativistic equations and determined the quasi-relativistic radial orbitals for every configuration group ( $4p^64d^N$ ,  $4p^54d^{N+1}$ ,  $4p^64d^{N-1}4f$ ,  $N = 1, 2, 3$ ) taking into account the correlation effects in the configuration interaction approximation. For this purpose, we have added the transformed radial orbitals with variable parameters to the basis of standard quasi-relativistic radial orbitals. These variable parameters were precisely specified to maximize the correction effects for the level energy. Further, we have created the basis of 38 radial orbitals by selecting the transformed radial orbitals with the principal quantum number  $n$  ranging from 5 to 8 and the orbital quantum number  $l$  acquiring all possible values. The set of all possible admixed configurations for one-electron and two-electron excitations from the shells with the principal quantum number  $n = 4$  was created by adopting this basis. Afterward the admixed configurations have been sorted out by their mean influence to the energy of the adjusted configurations by choosing the minimal value of statistical weights to be  $10^{-5}$ .

Table 6.1 shows the number of admixed configurations  $K$ , the initial number of configuration state functions  $C_0$  and the number of configuration state functions  $C_1$  determined after their reduction by using our selection methods for every configuration group in concern.

**Table 6.1** Admixed configuration numbers  $K$  and  $C$  for individual ions

<i>Ion</i>	<i>Adjusted configuration</i>	<i>K</i>	<i>C<sub>0</sub></i>	<i>C<sub>1</sub></i>
$W^{+37}$	$4p^64d^1$	37	11718	716
$W^{+37}$	$4p^54d^2, 4p^64f$	70	81092	32280
$W^{+36}$	$4p^64d^2$	43	47997	7019
$W^{+36}$	$4p^54d^3, 4p^64d4f$	82	290956	130370
$W^{+35}$	$4p^64d^3$	45	116686	30996
$W^{+35}$	$4p^54d^4, 4p^64d^24f$	93	698888	305019

It was proved that the use of the same basis could be very effective to get reliable results when the parameters of the electron-impact excitation were calculated. We are ready to include these

results to the data analysis system ADAS. In order to disseminate the results obtained during previous calculations, we have published the  $4p^64d^2$ ,  $4p^54d^3$  and  $4p^64d4f$  configuration spectrum characteristics of the  $W^{+36}$  ion in ADNDT journal (level energies, electric E1, E2, E3 and magnetic M1, M2 transition wavelengths  $\lambda$  and radiative transition probabilities  $A$ , radiative lifetimes  $t$ , etc.).

Additionally, by participating in the program “Establishing and development of atomic data base for astrophysical, technological and laboratory plasma modelling”, we have investigated six tungsten ions with an open 4p shell.

An important effect was discovered during investigation of spectroscopic parameters for the  $W^{36+}$  and  $W^{35+}$  ions. There are some levels of excited configurations which can not decay to the ground configuration by way of E1 transitions. Such transitions are forbidden by selection rules for total momentum  $J$ . To determine radiative lifetimes for these levels, one usually computes M1 and E2 transition probabilities. As our calculations have demonstrated, this is not enough. Some of these levels have relatively strong M2 and E3 transitions down to the ground configuration. Inclusion of such transitions for the radiative lifetime calculations can decrease lifetime values several times or even a dozen times. Keeping that in mind, we have investigated the dependence of radiative lifetimes on M2 and E3 transition probabilities for the particular levels of  $4p^54d^{N+1}+4p^64d^{N-1}4f$  configurations.

## 6.2 The evaluation of the accuracy of the theoretical investigation of ions with the different ionization degrees

For evaluation of the accuracy of the theoretical investigation of ions with the different ionization degrees the series of oxygen-like ions were taken. A recently developed and published new version of GRASP2K package was used [6.1] in which old spin-angular integration library has been replaced by the LIBRANG angular package developed by Mr. Gaigalas of VU ITPA based on the theory of [6.2, 6.3]. Tests of the new program have shown that errors encountered by NJGRAF do not occur with the new angular package.

The investigation of accuracy of the method and the program based on relativistic wave functions from multiconfiguration Dirac-Hartree-Fock (MCDHF) and configuration interaction (CI) calculations, E1, M1, E2, M2 transition rates, weighted oscillator strengths, and lifetimes are evaluated for the states of the  $(1s^2)2s^22p^4$ ,  $2s^2p^5$ , and  $2p^6$  configurations in all oxygen-like ions between F II and Kr XXIX [6.4]. Valence and core-valence correlation effects were taken into account by using single-double multireference (SD-MR) expansions to increasing sets of active orbitals.

Computed in this work energies agree very well with the experimental values, with differences between 300 and 600  $\text{cm}^{-1}$  for the majority of the ions in the sequence. Some possible problems with experimental identification of lines in As XXVI, Se XXVII, and Br XXVIII have been pointed out. The energy levels for these three spectra, presented in this work, agree much better with the Edlén [6.5] values than with NIST databases (results for these ions are based on Kelly [6.6]) (see Table 6.2). Our energy level calculations are considerably more accurate than other calculations (except for Vilkas and Ishikawa [6.7]).

There are excellent agreements with the most accurate multiconfiguration Dirac-Hartree-Fock calculations with the relativistic corrections in the Breit-Pauli approximation (MCHF-BP) at the low  $Z$  as well as with experimental lifetimes (Table 6.3).

From the results obtained in this work we can conclude that our calculations based on the MCDHF and CI approximations can serve as benchmark calculations for transition probabilities for the  $2s^22p^4$ ,  $2s^2p^5$ , and  $2p^6$  configurations of the oxygen-like sequence without the need for observed transition energies. The results of this work were published in paper [6.4]. The analysis has shown that errors encountered by NJGRAF do not occur with the new angular package from the new version of GRASP2K [6.1].

**Table 6.2** Comparison of fully relativistic theoretical energy levels with values derived from observed and semi-empirical (SE) wavelengths

As XXVI									
$2s^22p^4\ ^3P$	2	0	0	0	0	0			
	0	137 320	136 385	135 600	-1720	-785			
	1	281 330	281 802	281 734	404	-68			
$2s^22p^4\ ^1D$	2	377 300	376 598	376 586	-714	-12			
$2s^22p^4\ ^1S$	0	726 580	726 315	726 071	-509	-244			
$2s^2p^5\ ^3P^o$	2	1 403 750	1 404 724	1 404 572	822	-152			
	1	1 550 530	1 551 663	1 551 701	1171	38			
	0	1 716 190	1 717 549	1 717 342	1152	-207			
$2s^2p^5\ ^1P^o$	1	1 962 370	1 962 613	1 963 325	955	712			
$2p^6\ ^1S$	0		3 195 915	3 197 391		1476			
Se XXVII									
$2s^22p^4\ ^3P$	2	0	0	0	0	0			
	0	147 760	144 941	143 818	-3942	-1123			
	1	323 690	324 396	324 328	638	-68			
$2s^22p^4\ ^1D$	2	422 380	421 316	421 279	-1101	-37			
$2s^22p^4\ ^1S$	0	814 600	814 628	814 253	-347	-375			
$2s^2p^5\ ^3P^o$	2	1 488 420	1 489 811	1 489 560	1140	-251			
	1	1 649 100	1 650 791	1 650 866	1766	75			
	0	1 845 030	1 847 080	1 846 742	1712	-338			
$2s^2p^5\ ^1P^o$	1	2 090 120	2 091 234	2 091 988	1968	754			
$2p^6\ ^1S$	0		3 379 728	3 381 432		1704			
Br VVVIII									
$2s^22p^4\ ^3P$	2	0	0	0	0	0	0	0	0
	0	218 800	153 478	151 954	-66 846	-1524	152 035	-66 765	-1443
	1	379 800	371 663	371 606	-8 194	-57	371 858	-7942	195
$2s^22p^4\ ^1D$	2	483 040	470 699	470 643	-12 397	-56	470 804	-12 236	105
$2s^22p^4\ ^1S$	0	944 150	912 501	911 968	-32 182	-533	912 282	-31 868	-219
$2s^2p^5\ ^3P^o$	2		1 579 903	1 579 537		-366	1 580 945		1042
	1		1 755 028	1 755 196		168	1 756 684		1656
	0		1 986 274	1 985 784		-490	1 987 396		1122
$2s^2p^5\ ^1P^o$	1		2 229 358	2 230 149		791	2 231 636		2278
$2p^6\ ^1S$	0		3 573 416	3 575 415		1999	3 579 486		6070

**Notes.** The difference of theoretical energies from observed (Diff. (1)) and SE (Diff.(2)) ones are given (in  $\text{cm}^{-1}$ ). Primary data source for As XXVI, Se XXVII and Br XXVIII ions at NIST is from Kelly [6.6].

**References.** (a) Kramida et al. [6.8]; (b) Edlén [6.5]; (c) present calculations; (d) Vilkas et al. [6.7].

**Table 6.3 Comparison of lifetimes (in ms)**

<i>Ion</i>	<i>State</i>	$\tau_{RCI}^a$	$\tau_{MCHF-BP}^b$	$\tau_{exp}$
F II	$2s^2 2p^4 \ ^1S_0$	397.8	430.22	$420 \pm 12^c$
Ne III	$2s^2 2p^4 \ ^1S_0$	206.5	216.73	$223 \pm 11^d$ $213 \pm 4^e$
Si VII	$2s^2 2p^4 \ ^1S_0$	63.87	63.341	$63.6 \pm 0.7^f$
P VIII	$2s^2 2p^4 \ ^1D_2$	28.69	28.332	$28.63 \pm 0.08^g$
S IX	$2s^2 2p^4 \ ^1D_2$	13.74	13.510	$13.79 \pm 0.05^g$
Ar XI	$2s^2 2p^4 \ ^3P_1$	14.97	14.560	$14.8 \pm 1.1^h$

**References.** (a) Present calculations; (b) Froese Fischer & Tachiev [6.9]; (c) Calamai et al. [6.10]; (d) Daw et al. [6.11]; (e) Träbert et al. [6.12]; (f) Träbert et al. [6.13]; (g) Träbert et al. [6.14]; (h) Yang et al. [6.15].

### 6.3 Multiconfiguration Dirac-Hartree-Fock energy levels and transition probabilities for $W^{38+}$

To obtain the wavelengths and intensities of the prominent lines in electron-beam ion-trap (EBIT) spectra of Rb-like  $W^{37}$  to Cu-like  $W^{45}$  ions have been measured by Utter et al. [6.16]. In their paper the identification of lines depended on theoretical predictions of wavelengths from *ab initio* calculations performed by Fournier [6.17] using a fully relativistic parametric potential code. Quantum electrodynamic (QED) corrections were not included.

In the present work the calculation was done using multiconfiguration Dirac-Hartree-Fock (MCDHF) approximation using recently developed and published new version of GRASP2K package [6.1]. As a final step, a relativistic configuration interaction (RCI) calculation was performed to include the transverse-photon (Breit) interaction describing the transversely polarized photon contribution to the electron-electron interactions in the Coulomb gauge, the vacuum polarization (VP), and the self-energy (SE) corrections.

The MCDHF calculations were performed with the wave function expanded in a basis of CSFs defined in terms of orbitals that are coupled in *jj*-coupling. The level notations have been converted to LSJ coupling scheme using the newly developed JJ2LSJ program, part of the latest version of the GRASP2K code [6.1].

Table 6.4 contains the spectroscopic parameters for the electric dipole (E1) transitions from the  $4p^6 \ ^1S (J = 0)$  to the odd ( $4p^5 4d, 4p^5 5s$  with  $J = 1$ ) levels. The accuracy indicator of a transition probability,  $A_{ki}$ , is  $\delta T = |S_\ell - S_v| / \max(S_\ell, S_v)$ , where  $S_\ell$  is the line strength in the length and  $S_v$  in the velocity form. The  $\delta T$  values presented in Table 6.4 ( $\delta T \leq 0.0004$ – $0.0555$ ) indicate, that our results are sufficiently accurate.

Table 6.5 compares theoretical [6.17, 6.18], measured [6.16, 6.18] and present wavelengths. This table shows that our computed wavelengths agree well with observed wavelengths.

**Table 6.4** Transition data for E1 transitions from  $4p^6\ ^1S$  to selected upper levels with ( $J = 1$ ), wavelengths  $\lambda$  in Å, line strength  $S$  (length form), weighted oscillator strength  $f$  (length form), transition rate  $A_{ki}$  (length form) in  $s^{-1}$ ,  $\delta T$  accuracy indicator. Numbers in brackets represent the powers of 10

<i>Upper</i>	$\lambda$ (Å)	$S$	$gf$	$A_{ki}$ ( $s^{-1}$ )	$\delta T$
$4p^5 4d\ ^3P$	80.68	2.036[-3]	7.666[-3]	2.619[9]	0.0555
$4p^5 4d\ ^3D$	63.64	2.397[-1]	1.144	6.281[11]	0.0074
$4p^5 4d\ ^1P$	46.45	3.337[-1]	2.182	2.248[12]	0.0004
$4p^5 5s\ ^1P$	18.42	3.160[-2]	5.211[-1]	3.415[12]	0.0004
$4p^5 5s\ ^3P$	16.22	8.478[-3]	1.588[-1]	1.342[12]	0.0067

**Table 6.5.** Comparison of computed wavelengths ( $\lambda$  in Å) from different theories with observed wavelengths for transitions from  $4p^6\ ^1S$  to selected upper levels with ( $J = 1$ )

<i>Upper</i>	<i>Theo. [5.17]</i>	<i>Theo. [5.18]</i>	<i>Expt. [5.18]</i>	<i>Expt. [5.16]</i>	<i>This work</i>
$4p^5 4d\ ^3P$	80.8856	80.897		80.6420	80.68
$4p^5 4d\ ^3D$	63.3262	63.249	63.98	63.8834	63.64
$4p^5 4d\ ^1P$	46.1417	46.064	46.40	46.6703	46.45
$4p^5 5s\ ^1P$	18.3994	–	–	–	18.42
$4p^5 5s\ ^3P$	16.1941	–	–	–	16.22

## 6.4 Application of the analogues of relativistic integrals in R-matrix method for highly charged tungsten ions

### 6.4.1 Introduction

In order to obtain emission-line spectra or energy losses from plasma impurities, one needs to solve the balance equation which determines level populations for the ions of different ionization stages. In its turn, the balance equation requires a detailed knowledge of accurate atomic data describing atomic structure (energy levels, radiative transition probabilities, Auger transition rates) and photon or charged particle scattering from the ionized atoms.

The scattering problem has to do with all different processes that can occur after collision of a photon or charged particle with an ion. Both theoretical and experimental methods of obtaining scattering parameters are very complicated, especially when dealing with heavy and/or highly charged ions. Consequently, there is a real need for the sophisticated theoretical methods allowing to simplify or to reduce calculations required for a large scale scattering data generation unavoidable in plasma modelling database realization.

There exist several theoretical methods to calculate the cross sections necessary for practical applications. One of the most accurate and suitable techniques to solve the scattering problem is the R-matrix method. This method includes nearly all of the physical effects that contribute to cross sections and is applicable to all kinds of atoms, from neutral ones to highly ionized stages.

These calculations are prohibitively large and extremely time-consuming if performed in the relativistic coupling using, for example, the Dirac–Fock R-matrix method, because the accuracy of results depends on the number of target levels included (which is significantly larger compared to a non-relativistic LS-term case). On the other hand, the methods based on transformation of S- and K-matrices, calculated in the pure LS-coupling, to intermediate coupling can help to overcome the problem, because the number of terms is significantly smaller than the number of corresponding fine-structure levels making these terms. On the negative side, only the non-relativistic wave functions (and, consequently, non-relativistic interaction integrals) are used in the LS-coupling. This kind of approximation becomes unsuitable and unsustainable when one has to deal with the highly charged heavy ions where it is extremely important to use the relativistic wave functions and the suitable relativistic approximations.

We have developed an approach based on the analogues of the relativistic integrals (ARI) which enables one to utilize relativistic wave functions obtained in the Dirac–Fock approximation. By this both the direct and indirect relativistic effects are included in the final result. The direct effects arise when the masses of electrons increase due to the speed of electrons, and the electrons are pushed closer to the nucleus. Since the inner electrons move with larger speeds than outer ones, their mean distance from the nucleus changes more notably when compared with the mean distances obtained in non-relativistic calculations. Therefore, the inner electrons screen the charge of the centrally placed nucleus more effectively. Due to this screening, the outer electrons are pushed away from the nucleus inducing the indirect relativistic effects. The goal of the present research is an assessment of different R-matrix methods used in the calculations of atomic data for electron scattering from the highly charged tungsten ions and estimation of the importance of relativistic effects in the case of the electron-impact excitation from the outer shells of heavy ions. The collision strengths for the electron-impact excitation among the levels of the configurations with one electron in the outer 4s, 4p, 4d, 4f shells of  $W^{45+}$  are being determined when the different approaches to include the relativistic effects are adopted.

#### 6.4.2 Expressions for analogues of relativistic integrals

The main relations for analogues of relativistic integrals and methods used to find their expressions have been presented earlier. In the current work, we will present only the relations employed in our calculations with the R-matrix code which implements the intermediate coupling frame transformation (ICFT). The code includes one-electron integrals of operators for kinetic and potential energies in the field of the nucleus. The one-electron part of operators is extended by adding mass–velocity corrections and Darwin terms. All these relativistic corrections are replaced by general expressions for one-electron integrals:

$$I(n\ell, n'\ell) = \frac{1}{4\ell + 2} \sum_j [j] I(n\ell, n'\ell),$$

where  $I(n\ell, n'\ell)$  is a relativistic one-electron integral, which depends on large and small components of the relativistic single-electron wave functions  $P_{n\ell}(r)$  and  $Q_{n\ell}(r)$ . In the non-relativistic approximation, the one electron spin-orbit and the main part of spin-other-orbit interactions are taken into account using a spin-orbit constant.

#### 6.4.3 Results and discussion

As an initial step for the electron-ion scattering calculations, the basis of relativistic wave functions based on the Dirac–Fock type radial orbitals was determined. Relativistic wave functions were determined for the ground and the excited states with an outer electron in  $4\ell$  shells of the  $W^{45+}$  ions, when  $\ell = 0, 1, 2, 3$ . In the case of quasirelativistic calculations, the target orbitals were generated with the AUTOSTRUCTURE code (<http://amdpp.phys.strath.ac.uk/autos/>). Alternatively,

the GRASP0 code (<http://www.am.qub.ac.uk/DARC>) was adopted for the completely relativistic wave function calculation.

Using the obtained wave functions, we have calculated energy level spectra in a completely relativistic Dirac–Fock approach applying the configuration interaction (CI) method. This calculation includes all seven energy levels from the  $n = 4$  complex. The relativistic R-matrix calculation employing the regular scattering codes from the DARC program have been performed and electron-impact collision strength values were obtained. These data serve as a benchmark point for the comparison with the data obtained from the quasirelativistic R-matrix method based on the multichannel quantum defect theory and the intermediate coupling frame transformation with and without non-relativistic interaction integrals replaced by their relativistic versions.

**Table 6.6** Energy levels (in Ry) for the  $1s^22s^22p^63s^23p^63d^{10}4\ell$  ( $\ell = 0, 1, 2, 3$ ) configurations of  $W^{45+}$  obtained with the relativistic R-matrix code (DARC), quasirelativistic R-matrix code (ICFT), and quasirelativistic R-matrix code that uses the relativistic analogues of integrals (ARI). Results of 25-level calculation are noted as GRASP25

<i>Index</i>	<i>Level</i>	<i>DARC</i>	<i>ICFT</i>	<i>ARI</i>	<i>GRASP25</i>
1	$4s_{1/2}$	-29529.183	-29271.875	-29528.5	–
2	$4p_{1/2}$	7.217	6.796	7.309	7.220
3	$4p_{3/2}$	14.729	12.810	14.715	14.733
4	$4d_{3/2}$	25.856	23.911	25.874	25.859
5	$4d_{5/2}$	27.470	25.468	27.458	27.474
6	$4f_{5/2}$	39.328	37.762	39.332	39.331
7	$4f_{7/2}$	39.747	38.283	39.738	39.751

The calculation results obtained for the energy levels in the  $W^{45+}$  ion using three different approaches are presented in Table 6.6. One can say with certainty that results which include relativistic Dirac–Fock functions agree very well. The difference between their energies does not exceed 0.8 Ry for absolute energy values. If compared with respect to the ground  $4s_{1/2}$  level, the energies agree within 0.02 Ry, except for the largest discrepancy of 0.1 Ry determined for the  $4p_{1/2}$  level.

The fine-structure splitting for the considered configurations agree even better. It is worth to notice that spin-orbit splitting between levels of  $4\ell_{1-1/2}$  and  $4\ell_{1+1/2}$  configurations is smaller in calculations which employ analogues of relativistic integrals than the splitting values obtained from the fully relativistic approach. It means that our spin-orbit constant provides underestimated values. The largest disagreement of 0.11 Ry is obtained for the  $4p$  configuration levels while discrepancy for the  $4f$  configuration levels does not exceed 0.02 Ry. On the other hand, the quasirelativistic approach gives deviation from relativistic calculations for spin-orbit splitting of 1.5 Ry for the  $4p$  configuration, while for the  $4f$  configuration, the splitting is larger by approximately 0.1 Ry. This confirms the fact that indirect relativistic effects are taken into account when relativistic wave functions are obtained by solving Dirac–Fock equations. Furthermore, all absolute values of the level energies are higher in quasirelativistic calculations than the calculated relativistic energies by approximately 257 Ry. Agreement for the energies relative to the ground level is much worse in this case too.

Our calculated energy levels are compared to the relativistic calculation data taken from [6.12]. In the latter study, 25 levels of  $W^{45+}$  were included in the target wave function CI expansion in order to perform relativistic R-matrix calculation. It is evident from Table 6.6 that the data from our completely relativistic calculation (DARC) are of the same quality as those from relativistic DARC calculations.

The data for collision strengths obtained using different approaches for three transitions in  $W^{45+}$  ions are presented in Figure 6.1 – Figure 6.3. We have adopted 1.6 a.u. R-matrix radius in all three calculations which included 25 continuum orbitals for each channel angular momentum in the expansion of the wave function. In the DARC calculations, the target consist of 7 levels, the maximum number of channels for a partial wave is 32, and the size of the corresponding Hamiltonian matrix is 808. In the non-relativistic scattering calculations without and with analogues of relativistic integrals, the target has 4 terms, the maximum number of channels is 10, and the size of the corresponding Hamiltonian matrix is 250. We have included all partial waves with angular momentum  $J \leq 29$  in all three cases. No top-up procedures are taken into account. It can be seen that the resonance structure in DARC and ARI cases is very similar. Some differences can

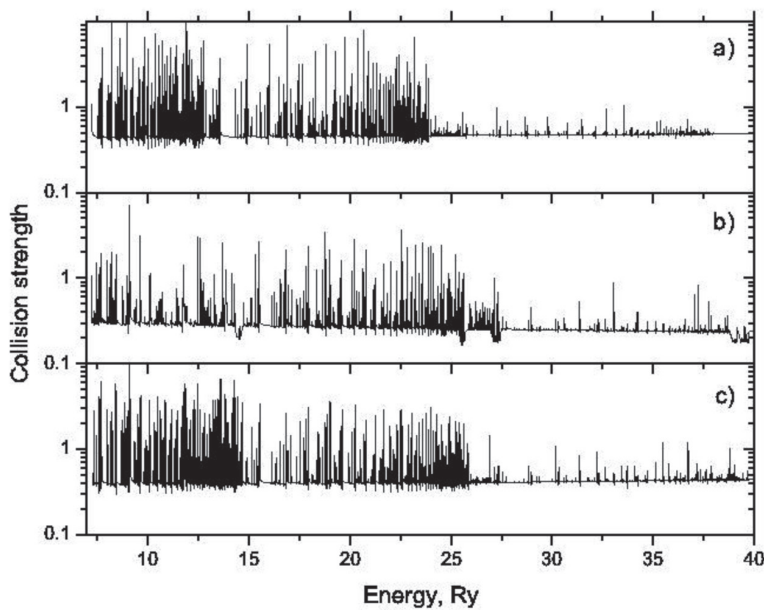


**Figure 6.1**

Electron-impact excitation collision strengths for the  $4s_{1/2} - 4p_{1/2}$  transition in  $W^{45+}$ . Data have been obtained with (a) the quasirelativistic R-matrix code (ICFT), (b) the relativistic R-matrix code (DARC), and (c) the same quasirelativistic R-matrix code with the relativistic analogues of integrals adopted

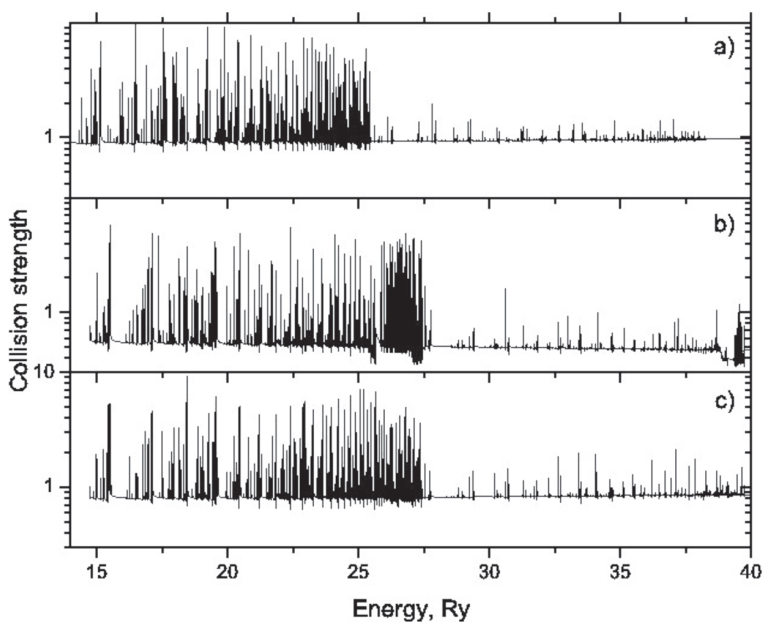
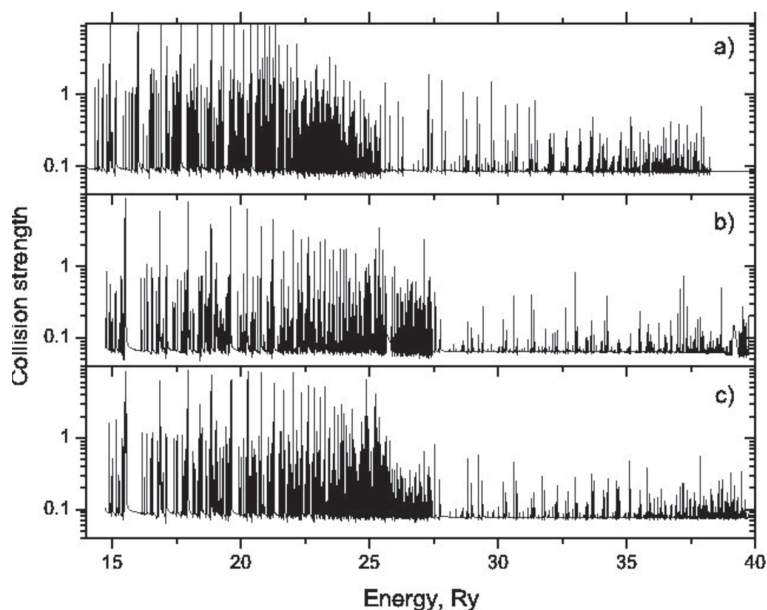


**Figure 6.2**

Electron-impact excitation collision strengths for the  $4s_{1/2} - 4p_{3/2}$  transition in  $W^{45+}$ . Data have been obtained with (a) the quasirelativistic R-matrix code (ICFT), (b) the relativistic R-matrix code (DARC), and (c) the same quasirelativistic R-matrix code with the relativistic analogues of integrals adopted

**Figure 6.3**  
Electron impact excitation collision strengths for the  $4p_{1/2}-4p_{3/2}$  transition in  $W^{45+}$ . Data have been obtained with (a) the quasirelativistic R-matrix code (ICFT), (b) the relativistic R-matrix code (DARC), and (c) the same quasirelativistic R-matrix code with the relativistic analogues of integrals adopted



be explained by the different energy mesh employed in the codes. Although agreement between various relativistic data is good, the collision strengths obtained with the ARI approach are slightly higher than those calculated in the completely relativistic (DARC) approximation. The reason of the differences is not clear so far. One can notice some prominent 'dips' in collision strength values calculated using the DARC code for the excitation to  $4p_{1/2}$  and  $4p_{3/2}$  levels at incident electron energies close to 25 Ry. These irregularities can be attributed to the malfunctioning of this code for the outer region.

In Table 6.7, we present effective collision strengths for the 1–2, 1–3, and 2–3 excitations in the  $W^{45+}$  ion. A good agreement between two relativistic approaches is evident at low temperatures, where the resonance contribution makes the most part of effective collision strengths. For all three excitations, effective collision strengths increase with the temperature increasing in ARI case, while their values from ICFT calculations have a decreasing character. On the other hand, DARC values show a slightly increasing tendency. The reason of these differences is still unclear.

**Table 6.7** Comparison of effective collision strengths for the  $4s_{1/2}-4p_{1/2}$ ,  $4s_{1/2}-4p_{3/2}$ , and  $4p_{1/2}-4p_{3/2}$  excitations in the  $W^{45+}$  ion determined using the quasirelativistic R-matrix code (ICFT), fully relativistic R-matrix code (DARC), and analogues of relativistic integrals (ARI) method

<i>T(K)</i>	$4s_{1/2}-4p_{1/2}$			$4s_{1/2}-4p_{3/2}$			$4p_{1/2}-4p_{3/2}$		
	<i>ICFT</i>	<i>DARC</i>	<i>ARI</i>	<i>ICFT</i>	<i>DARC</i>	<i>ARI</i>	<i>ICFT</i>	<i>DARC</i>	<i>ARI</i>
500	0.68	0.45	0.48	1.15	0.51	0.87	0.24	0.11	0.11
750	0.69	0.51	0.54	1.14	0.55	0.95	0.23	0.11	0.12
1000	0.69	0.56	0.57	1.12	0.56	0.99	0.21	0.11	0.12
1500	0.69	0.59	0.61	1.09	0.58	1.04	0.19	0.11	0.12
2000	0.70	0.61	0.63	1.06	0.59	1.06	0.18	0.11	0.13
3000	0.70	0.59	0.65	1.02	0.60	1.08	0.16	0.12	0.13
5000	0.70	0.54	0.65	0.98	0.60	1.10	0.14	0.12	0.13
7500	0.70	0.49	0.64	0.96	0.59	1.11	0.13	0.12	0.15
10000	0.70	0.46	0.64	0.95	0.59	1.13	0.13	0.12	0.15

We can make several observations and conclusions from performed comparisons. For highly and heavy elements, the relativistic wave functions have to be employed in atomic calculations. The approach where non-relativistic integrals are substituted for their relativistic analogues extends possible application of available computer codes. A fairly good agreement with Dirac–Fock values is obtained for the energy levels of  $1s^2 2s^2 2p^6 3s^2 3p^6 3d^{10} 4\ell$  ( $\ell = 0, 1, 2, 3$ ) configurations of  $W^{45+}$  ion when calculations are performed with relativistic analogues of integrals. However, the data from quasirelativistic approximation employing corresponding wave functions exhibit larger discrepancies. The difference from relativistic energies is approximately 257 Ry for the absolute values of energies. Furthermore, the applied quasirelativistic approach overestimates the spin-orbit splitting for the considered configurations. This demonstrates the fact that the indirect relativistic effects are taken into account with relativistic two-component radial wave functions when valence electrons are more effectively screened from the nucleus. Consequently, they are pushed away from the nucleus, and their velocities decrease. This affects the value of the spin-orbit constant as well. In general, the quasirelativistic calculations slightly overestimate collision strengths if compared with the approaches where relativistic wave functions are used.

## 6.5 References

- 6.1. Z.R. Rudzikas. *Theoretical Atomic Spectroscopy*. Cambridge University Press, 2nd ed. 2007.
- 6.2. G. Gaigalas, Z. Rudzikas, P. Rynkun, A. Alkauskas. *Phys. Rev. A*, **83**, 032509 (2011).
- 6.3. P. Jonsson, X. He, C. Froese Fischer, I.P. Grant. *Comput. Phys. Commun.*, **177**, 597 (2007).
- 6.4. B. J. McKenzie, I. P. Grant, P. H. Norrington. *Comput. Phys. Commun.*, **21**, 233 (1980).
- 6.5. C. Froese Fischer, G. Gaigalas, Y. Ralchenko. *Comput. Phys. Commun.*, **175**, 738 (2006).
- 6.6. F. M. Gu. Flexible Atomic Code, <http://kipac-tree-stanford.edu/fac>.
- 6.7. <http://www.efda.org/newsletter/efficient-high-power-plasma-heating/>
- 6.8. Nick Hollpway. MAST reaps the benefits of international collaboration, *Fusion in Europe*, No. 1, 5 (2012).
- 6.9. J. Slater, F. H. Read, S. E. Novik, W. C. Lineberg. Alkali negative ions: III. Multichannel photodetachment study of Cs<sup>-</sup> and K<sup>-</sup>. *Phys. Rev. A*, **17**, 201 (1978).
- 6.10. A. R. Johnston, P. D. Burrow. Temporary negative-ion states of Na, K, Rb and Cs. *Phys. Rev. A*, **59**, 406 (1995).
- 6.11. A. A. Borovik, O. Zatsarinny, K. Bartchat. Resonance effects in electron and photon impact excitation of the p<sub>6</sub> subvalence subshell in alkali atoms. *J. Phys. B*, **42**, 044010 (2009).
- 6.12. A. Kupliauskienė. Theoretical study of the  $5p^5 nln'l'$  autoionizing states of Cs, *Physica Scripta*, **84**, 045304 (7pp) (2011).
- 6.13. V. Pejcev, K. J. Ross. *J. Phys. B: At. Mol. Phys.*, **10**, 2935 (1977).
- 6.14. E. Träbert, M. Grieser, J. Hoffmann, C. Krantz, R. Repnow, A. Wolf. *Phys. Rev. A* **85**, 042508 (2012).
- 6.15. L. Yang, D. A. Church, S. Tu, J. Jin. *Phys. Rev. A* **50**, 177 (1994).
- 6.16. S. B. Utter, P. Beiersdorfer, E. Träbert, *Can. J. Phys.* **80**, 1503 (2002).
- 6.17. K. B. Fournier, *Atomic Data and Nuclear Data Tables* **68**, 148 (1998).
- 6.18. R. Radtke, C. Biedermann, G. Fussmann, J. I. Schwob, P. Mandelbaum, R. Doron, *Atomic and Plasma Material Interaction Data for Fusion* **13**, 45 (2007).

## 7 MOBILITY PROGRAM 2013

During 2013 the following visits were implemented under the mobility plan:

### Fusion safety issues

**Mr. E. Urbonavičius, Mr. G. Dundulis, Mr. R. Alzbutas and Mr. T. Kaliatka** visited **Max-Planck-Institut für Plasmaphysik (IPP)** in Greifswald (Germany) in the period **2013/12/15 – 2013/12/18**. At first a visit to facility W7-X was paid to see the current status of the W7-X facility. Together with Mr. D. Naujoks the co-operation activities in 2013 and plans for 2014 were discussed. In discussions with Mr. D. Naujoks it was agreed on the list of topics that need to be considered in 2014 as necessary for further investigations. However, it was noted that EFDA project finishes in by the end of 2013, and another forms of cooperation will have to be identified in future. Detailed agreement will be reached later in 2014.

**Mr. E. Urbonavičius** presented results received with COCOSYS code for assessment of plasma vessel pressure build-up in case of 40 mm pipe rupture during “baking” mode operation. The analysis was performed taking into account the location of in-vessel components. Result showed that the capacity of planed burst disc is enough to ensure protection of the vessel.

**Mr. G. Dundulis** presented the report on structural integrity analysis of W7-X components performed during 2013. The load scale limit analysis results to failure of the welding connections for ports AEK20 and the PV shell with gap 1 mm are presented. This analysis was performed using ABAQUS code. According to the results of analysis, it is possible to conclude that the stability of the welding between Plasma Vessel and ports AEK20 will be sustained to end value of load scaling factor (SF = 6.0).

The FE models prepared for pipes whip impacts analysis on neighbouring piping and structures inside and outside plasma vessel (PV), and primary analysis of pipe displacement for whip analysis outside PV (outPV) are presented in this report. The main purposes of pipe displacement analysis evaluate the possible displacement of pipe in case of guillotine rupture and estimate possible impact to neighbouring structures. For the pipe displacement evaluation Peps software was used.

**Mr. R. Alzbutas** presented the results of Reliability Analyses of the Divertor Target Cooling Circuit ACK10 & Plasma Vessel / Ports Cooling Circuit ABK10 to be considered for further application in the W7-X facility design.

**Mr. T. Kaliatka** presented the results of thermo-hydraulic analyses of the W7-X plasma vessel venting system in case of LOCA in “baking” mode were presented. Different level of blockage in the venting system was analysed. Analysis showed that 35 mm diameter is enough to prevent overpressure. Also results of vacuum pump application to avoid burst disk opening in case of small leaks in plasma vessel was presented. Results showed that the existing vacuum pump capacity is sufficient to prevent the pressure rise in plasma vessel if break of cooling system is less than 6 mm<sup>2</sup>.

### Technology development burning plasmas

**Mr. G. Stankūnas** visited **CSU-Garching on 2013/04/08 – 2013/04/10** to participate at the kick-off meeting of WP13-SYS02 “System level analysis”. At the meeting, detailed activities were discussed among the participants. In the WP13-SYS02-T08 there are three associations involved:

CIEMAT, KIT, and LEI. The aim of the task is to use MCNP coupled with FISPACT/EAF to calculate the activation and decay heat production of the in-vessel components. For the HCLL options, just the structural material has to be exchanged: Eurofer by high temperature ferritic martensitic steel and by 316L(N) and this will be done by LEI.

The Final meeting of WP13-SYS02 “System level analysis” was held at **CSU-Garching on 2013/12/03 – 2013/12/05**, where **Mr. G. Stankūnas** discussed the achieved results and possible further activities in the field.

**Mr. R. Alzbutas** and **Mr. T. Iešmantas** participated at the **kick-off meeting of task area WP13-DTM02 “DEMO RAMI tools & methodologies”**, which was held at **CSU-Garching** during **2013/04/11 – 2013/04/13**. Mr. R. Alzbutas discussed activities in WP13-DTM02-T04 “Analysis of the DEMO Availability Requirement” and Mr. T. Iešmantas discussed activities in WP13-DTM02-T02 “Method to evaluate and integrate diverse RAMI input data”.

A detailed work plan was discussed and agreed upon among the participants. Work plan for the task WP13-DTM02-T04 “Analysis of the DEMO Availability Requirement” was presented for other participants. In LEI (Lithuanian Energy Institute) we were expecting to be involved in the project sharing our experience on RAMI (including activities in WP12, namely “Expected initial availability and availability growth of the DEMO plant based on historical data”) and requirements development for PSA (Probabilistic Safety Assessment). For analysis of the DEMO Availability Requirement the proposed activities focused on:

- a. Identification of relevant measures and suitable parameters of Availability Requirement to reflect the actual efficiency (including economic output) of the DEMO facility.
- b. Demonstration/modelling and clarification of various definitions and alternatives considering different measures and parameters of Availability Requirement for DEMO.
- c. Analysis of selected DEMO Availability Requirement taking into account energy sector industry practice and further developed DEMO specific pulse-operation scheme.

Work plan for the task WP13-DTM02-T02 “Method to evaluate and integrate diverse RAMI input data” was presented for other participants. LEI owned software REPEAT as well as RAMI data sources (like T-Book, MIL-HDBK-217F, Bellcore/Telcordia, NSWC Mechanical components) was presented as “to be used” in the development of RAMI data analysis methodology.

The **Final meeting of WP13-DTM02 “DEMO RAMI tools & methodologies”** was held at **CSU-Garching on 2013/12/11 – 2013/12/13**, where **Mr. R. Alzbutas** and **Mr. T. Iešmantas** discussed the achieved results and possible further activities in the field.

**Mr. E. Urbonavičius** participated at the **interim meeting of WP13-SYS04 “Safety”**, which was held in the premises of **CSU-Garching** during **2013/09/23 – 2013/09/25**. The results already achieved and plans for completion of the tasks were discussed and agreed upon among the participants. LEI participates in activities of WP12-SYS04-T05 “Report on tools for safety studies”, which is coordinated by ENEA.

The final meeting of **WP13-SYS04 “Safety”** was held in the premises of **CSU-Garching** during **2013/12/02 – 2013/12/04**. At the meeting **Mr. E. Urbonavičius** made a presentation of WP12-SYS04-T05 draft final report. Participants of the meeting discussed already achieved results and plans for completion of the tasks.

**Mr. E. Urbonavičius** and **Mr. G. Stankūnas** participated at the EFDA information meeting, which was held at **CSU-Garching** during **2013/10/28 – 2013/10/31**. At the EFDA information meeting the announced Calls for Participation in work plan 2014-2018 tasks were discussed among the participants. At the meeting the information about the new rules for participation in fusion research activities were presented by the project coordinators. The expression of interest to participate in the fusion activities has to be submitted via ECOM system before 2013/11/12. E. Urbonavičius had most interest in safety analysis and thermal-hydraulic analysis, while G. Stankūnas concentrated his attention on neutronic analysis for DEMO.

**Mr. G. Stankūnas** visited **CSU – Culham (CCFE)** during **2013/11/04 – 2013/11/06** to participate at the EFDA information meeting. The meeting announced Calls for Participation in work plan 2014-2018 tasks were discussed among the participants. At the meeting the information about the new rules for participation in fusion research activities were presented by the project coordinators. The expression of interest to participate in the fusion activities has to be submitted via ECOM system before 2013/11/12. A special interest is studies in the field of neutronic analysis at JET.

### Meetings under EFDA:

**Mr. G. Stankūnas** visited **CSU – Culham (CCFE)** during **2013/06/11 – 2013/06/14** in the frames of Fusion technology task force (TF-FT) to participate in the EFDA JET monitoring meeting. Together with dr. Paola Batistoni the activities in 2013 were discussed and semi-annual meeting presentation was presented. Some issues were identified regarding availability of final neutron spectra. It was agreed that after spectrum from D1 will be available, to continue on deliverable D2 – Calculation of activation coefficients and comparison; assessment of related uncertainties. In parallel – Calculation of activation coefficients for reviewed activation reactions with energy threshold in the range 3–14 MeV and continuation on the preparation of the final report.

## 8 PUBLIC INFORMATION

The information related to FUSION energy perspectives, last achievements in ITER development and other Fusion research fields is continuously distributed among universities, R&D institutions, schools:

All activities which were organised in Lithuanian Energy Institute are mentioned (with photos, presentations) on the web-site of Lithuanian Energy Institute <http://www.lei.lt> in section "News" -> "News archive" (both in English and Lithuanian versions).

Information on FUSION and EURATOM-LEI activities is placed on the web-site of Lithuanian Energy Institute <http://www.lei.lt> in section "International projects" -> "EURATOM-LEI".

In 2013 annual classic PI activities were held:

- 10<sup>th</sup> International Conference of Young Scientists on Energy Issues (CYSENI). 29-31 May 2013. Keynote and section presentations on fusion.
- Carrier days at Kaunas University of Technology. 13 March 2013. Dissemination of material on fusion.

In 2013 there were the following specific activities to spread the information about the nuclear fusions and ITER project to public:

### Public paper in news portal

- A public paper "The part of most extreme experiment for Lithuanian scientists" <http://www.delfi.lt/mokslas/mokslas/lietuvos-mokslininkams-patiketa-ekstremaliausio-eksperimento-zemeje-dalis.d?id=64407004#iXzz2xc3iHW6X> (in Lithuanian) was prepared by Chief Specialist in Public Relations of the Lithuanian academy of science R. Maskoliūnas who was consulted by P. Bogdanovich of Vilnius University.

### Outreach and education

- The Club of young power specialists established by the students of Vilnius University are organising lectures about different energy issues. A. Kupliauskienė of VU ITPA gave a lecture "The perspectives of thermonuclear energy" at the meeting of this club at Vilnius University (Lithuania) on November, 2013.

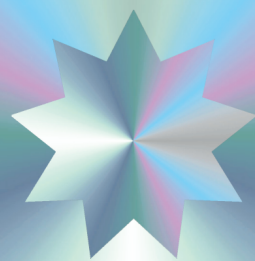
### Appearance in the media

- P. Bogdanovich gave an interview about nuclear fusion and ITER project for TV show "Science express" at national Lithuanian TV. The recorded interview is available at <http://www.delfi.lt/video/mokslas-ir-gamta/mokslo-expresas/mokslo-expresas-gilyn-i-atoma.d?id=64276878> (in Lithuanian). As well this interview is available at <http://www.youtube.com/watch?v=pCHWmudVhIE>.

## 9 PUBLICATIONS

- 9.1. Ušpuras E., Kaliatka A., Kaliatka T. Analysis of the accident with the coolant discharge into the plasma vessel of the W7-X fusion experimental facility. *Fusion engineering and design*. ISSN 0920-3796. 2013. Vol. 88, Iss. 5, p. 304-310.
- 9.2. Dundulis G., Janulionis R., Karalevičius R. The application of leak before break concept to W7-X target module. *Fusion engineering and design*. ISSN 0920-3796. 2013. Vol. 88, p. 307-313.
- 9.3. Kaliatka T., Ušpuras E., Kaliatka A. Analysis of processes in vacuum vessel during ingress of coolant event. The 15th inter-national topical meeting on nuclear reactor thermal-hydraulics (NURETH-15), Pisa, Italy, May 12-17, 2013, (CD), p. 1-8.
- 9.4. Kaliatka T. Analysis of thermal hydraulic processes during different operation modes of Wendelstein 7-X experimental fusion reactor,. 10<sup>th</sup> annual international conference of young scientists on energy issues (10 CYSENI anniversary): Kaunas, Lithuania, May 29-31, 2013. Kaunas: LEI, 2013. ISSN 1822-7554, p. 632-641.
- 9.5. Kaliatka T. Termobranduolinės sintezės įrenginiai pasaulyje. Šilumos energetika ir technologijos-2013: konferencijos pranešimų medžiaga, Kauno technologijos universitetas, 2013 m. sausio 31-vasario 1. Kaunas: Technologija, 2013. ISSN 2335-2477, p. 51-56.
- 9.6. Stankūnas G. Experimental study of p (1 GeV)+ natU fission-spallation reaction and delayed neutron measurements // *International journal of modern physics E Nuclear Physics*. ISSN 0218-3013. 2013. Vol. 22, Iss. 12, p. 1-12.
- 9.7. Stankunas G., Syme B., Popovichev S., Conroy S., Batistoni P., Safety analyses in support of neutron detector calibration operations. 11<sup>th</sup> International Symposium on Fusion Nuclear Technology, Barcelona, September 16-20, 2013.
- 9.8. Voronov R., Alzbutas R. Probabilistic reliability and risk analysis for systems of fusion device- Proceedings of the 20<sup>th</sup> advances in risk and reliability technology symposium (AR2TS), Loughborough, Leicestershire, May 21-23, 2013. Loughborough University, 2013. ISBN 978-1-907382611, p. 347-355.
- 9.9. Voronov R., Alzbutas R. Application of probabilistic safety and reliability analysis for a system of fusion facility // *Energetika*. ISSN 0235-7208. 2013. T. 59, Nr.4, p. 183-193.
- 9.10. Bogdanovich P., Kisielius R. Theoretical energy level spectra and transition data for  $4p^6 4d^2$ ,  $4p^6 4d 4f$ , and  $4p^5 4d^3$  configurations of W36+. *Atomic Data and Nuclear Data Tables*, 99, 580-594 (2013).
- 9.11. Karazija R., Kučas S. Average characteristics of the configuration interaction in atoms and their applications. *Journal of Quantitative Spectroscopy and Radiative Transfer*, 129, 131-144 (2013).
- 9.12. Jonauskas V., Kisielius R., Masys Š., Kynienė A. Analogues of relativistic integrals: their application in R-matrix method for highly charged tungsten ions. *Lith. J. Phys.*, 53, 144-149 (2013).
- 9.13. Karazija R., Kučas S., Jonauskas V., Momkauskaitė A. Formation of a narrow group of intense lines in the emission and photoexcitation spectra. In "New Trends in Atomic and Molecular Physics", Ed. M. Mohan, Springer Press, 2013, p. 167-188.

- 9.14. Bosch H.-S., Wolf R.C., Andreeva T., Baldzuhn J., Birus D., Bluhm T., Bräuer T., Braune H., Bykov V., Cardella A., Durodié F., Endler M., Erckmann V., Gantenbein G., Hartmann D., Hathiramani D., Heimann P., Heinemann B., Hennig C., Hirsch M., Holtum D., Jagielski J., Jelonnek J., Kasperek W., Klinger T., König R., Kornejew P., Kroiss H., Krom J.G., Kühner G., Laqua H., Laqua H.P., Lechte C., Lewerentz M., Maier J., McNeely P., Messiaen A., Michel G., Ongena J., Peacock A., Pedersen T.S., Riedl R., Riemann H., Rong P., Rust N., Schacht J., Schauer F., Schroeder R., Schweer B., Spring A., Stäbler A., Thumm M., Turkin Y., Wegener L., Werne A., Zhang D., Zilker M., Akijama T., Alzbutas R., Ascasibar E., Balden M., Banduch M., Baylard Ch., Behr W., Beidler C., Benndorf A., Bergmann T., Biedermann C., Bieg B., Biel W., Borchardt M., Borowitz G., Borsuk V., Bozhenkov S., Brakel R., Brand H., Brown T., Brucker B., Burhenn R., Buscher K-P., Caldwell-Nichols C., Cappa A., Cardella A., Carls A., Carvalho P., Ciupiński Ł., Cole M., Collienne J., Czarnecka A., Czymek G., Dammertz G., Dhard C.P., Davydenko V.I., Dinklage A., Drevlak M., Drotziger S., Dudek A., Dumortier P., Dundulis G., Eeten P.V., Egorov K., Estrada T., Faugel H., Fellingner J., Feng Y., Fernandes H., Fietz W.H., Figacz W., Fischer F., Fontdecaba J., Freund A., Funaba T., Fünfgelder H., Galkowski A., Gates D., Giannone L., García Regaña J.M., Geiger J., Geißler S., Greuner H., Grahl M., Groß S., Grosman A., Grote H., Grulke O., Haas M., Haiduk L., Hartfuß H.J., Harris J.H., Haus D., Hein B., Heitzenroeder P., Helander P., Heller R., Hidalgo C., Hildebrandt D., Höhnle H., Holtz A., Holzhauser E., Holzthüm R., Huber A., Hunger H., Hurd F., Ihrke M., Illy S., Ivanov A., Jablonski S., Jaksic N., Jakubowski M., Jaspers R., Jensen H., Jenzsch H., Kacmarczyk J., Kaliatka T., Kallmeyer J., Kamionka U., Karalevičius R., Kern S., Keunecke M., Kleiber R., Knauer J., Koch R., Kocsis G., Könies A., Köppen M., Koslowski R., Koshurinov J., Krämer-Flecken A., Krampitz R., Kravtsov Y., Krychowiak M., Krzesinski G., Ksiazek I., Kubkowska M., Kus A., Langish S., Laube R., Laux M., Lazerson S., Lennartz M., Li C., Lietzow R., Lohs A., Lorenz A., Louche F., Lubyako L., Lumsdaine A., Lysoivan A., Maaßberg H., Marek P., Martens C., Marushchenko N., Mayer M., Mendeleevitch B., Mertens Ph., Mikkelsen D., Mishchenko A., Missal B., Mizuuchi T., Modrow H., Mönnich T., Morizaki T., Murakami S., Musielok F., Nagel M., Naujoks D., Neilson H., Neubauer O., Neuner U., Nocentini R., Noterdaeme J.-M., Nührenberg C., Obermayer S., Offermanns G., Oosterbeek H., Otte M., Panin A., Pap M., Paquay S., Pasch E., Peng X., Petrov S., Pilopp D., Pirsch H., Plaum B., Pompon F., Povilaitis M., Preinhaelte J., Prinz O., Purps F., Rajna T., Récsé S., Reiman A., Reiter D., Rimmel J., Renard S., Rhode V., Riemann J., Rimkevičius S., Riße K., Rodatos A., Rodin I., Romé M., Roscher H.-J., Rummel K., Rummel Th., Runov A., Ryc L., Sachtleben J., Samartsev A., Sanchez M., Sano F., Scarabosio A., Schmid M., Schmitz H., Schmitz O., Schneider M., Schneider W., Scheibl L., Scholz M., Schröder G., Schröder M., Schruff J., Schumacher H., Shikhovtsev I.V., Shoj M., Siegl G., J. Skodzik J., Smirnow M., Speth E., Spong D.A., Stadle R., Sulek Z., Szabó V., Szabolics T., Szetefi T., Szökefalvi-Nagy Z., Tereshchenko A., Thomsen H., Thumm M., Timmermann D., Tittes H., To K., Tournianski M., Toussaint U., Tretter J., Tulipán S., Turba P., Uhlemann R., Urban J., Urbonavičius E., Urlings P., Valet S., Van Eester D., M. Van Schoor M., Vervier M., Viebke H., Vilbrandt R., Vrancken M., Wauters T., Weissgerber M., Weiß E., Weller A., Wendorf J., Wenzel U., Windisch T., Winkler E., Winkler M., Wolowski J., Wolters J., Wrochna G., Xanthopoulos P., Yamada H., Yokoyama M., Zacharias D., Zajac J., Zangl G., Zarnstorf M., Zeplien H., Zoletnik S., Zuin M. Technical challenges in the construction of steady-state stellarator Wendelstein 7-X // Nuclear fusion. ISSN 0029-5515. 2013. Vol. 53, No. 12, p. 1-16.



ISSN 2029-1612



9 772029 161000